Lawrence Berkeley National Laboratory

Lawrence Berkeley National Laboratory

Title

Evaluation of a deposit in the vicinity of the PBU L-106 Site, North Slope, Alaska, for a potential long-term test of gas production from hydrates

Permalink

https://escholarship.org/uc/item/0zv0776m

Author

Moridis, G.J.

Publication Date

2010-06-01

eScholarship.org Powered by the California Digital Library
University of California

Evaluation of a Deposit in the Vicinity of the PBU L-106 Site, North Slope, Alaska, for a Potential Long-Term Test of Gas Production From Hydrates

G.J. Moridis, SPE; M.T. Reagan, SPE; K. Boyle, and K. Zhang, SPE, Lawrence Berkeley National Laboratory

Abstract

As part of the effort to investigate the technical feasibility of gas production from hydrate deposits, a long-term field test (lasting 18-24 months) is under consideration in a project led by the U.S. Department of Energy. We evaluate a candidate deposit involving the C-Unit in the vicinity of the PBU-L106 site in North Slope, Alaska. This deposit is stratigraphically bounded by impermeable shale top and bottom boundaries (Class 3), and is characterized by high intrinsic permeabilities, high porosity, high hydrate saturation, and a hydrostatic pressure distribution. The C-unit deposit is composed of two hydrate-bearing strata separated by a 30-ft-thick shale interlayer, and its temperatrure across its boundaries ranges between 5 and 6.5 ^{o}C.

We investigate by means of numerical simulation involving very fine grids the production potential of these two deposits using both vertical and horizontal wells. We also explore the sensitivity of production to key parameters such as the hydrate saturation, the formation permeability, and the permeability of the bounding shale layers. Finally, we compare the production performance of the C-Unit at the PBU-L106 site to that of the D-Unit accumulation at the Mount Elbert site, a thinner, single-layer Class 3 deposit on the North Slope of Alaska that is shallower, less-pressurized and colder (2.3 – 2.6 ^{o}C). The results indicate that production from horizontal wells may be orders of magnitude larger than that from vertical ones. Additionally, production increases with the formation permeability, and with a decreasing permeability of the boundaries. The effect of the hydrate saturation on production is complex and depends on the time frame of production. Because of higher production, the PBU-L106 deposit appears to have an advantage as a candidate for the long-term test.

Introduction

Background. Gas hydrates (GH) are solid crystalline compounds of water and gaseous substances described by the general chemical formula G•N_H H_2O, in which the molecules of gas G (referred to as guests) occupy voids within the lattices of ice-like crystal structures. Hydrate deposits occur in two distinctly different geographic settings where the necessary conditions of low temperature T and high pressure P exist for their formation and stability: in the Arctic (typically in association with permafrost) and in deep ocean sediments (Kvenvolden, 1988).

The majority of naturally occurring hydrocarbon gas hydrates contain CH_4 in overwhelming abundance. Simple CH_4-hydrates concentrate methane volumetrically by a factor of ~164 when compared to standard P and T conditions (STP). Natural CH_4-hydrates crystallize mostly in the structure I form, which has a hydration number N_H ranging from 5.77 to 7.4, with $N_H = 6$ being the average hydration number and $N_H = 5.75$ corresponding to complete hydration (Sloan and Koh, 2008). Natural GH can also contain other hydrocarbons (alkanes C_nH_{2n+2}, n = 2 to 4), but may also contain trace amounts of other gases (mainly CO_2, H_2S or N_2).

Although there has been no systematic effort to map and evaluate this resource on a global scale, and current estimates of in-place volumes vary widely (ranging between 10^{15} to 10^{18} m^3 at standard conditions), the consensus is that the worldwide quantity of hydrocarbon GH is vast (Milkov, 2004; Klauda and Sandler, 2005; Sloan and Koh, 2008). Given the sheer magnitude of the resource, ever increasing global energy demand, and the finite volume of conventional fossil fuel resources, GH are emerging as a potential energy source for a growing number of nations. The attractiveness of GH is further enhanced by the environmental desirability of natural gas, as it is an energy resource with a significantly lower carbon intensity than coal, oil, or other solid and liquid fuels. Thus, the appeal of GH accumulations as future hydrocarbon gas sources is rapidly increasing and their production potential clearly demands technical and economic evaluation. The past decade has seen a marked acceleration in gas hydrate R&D, including both a proliferation of basic scientific endeavors as well as the strong emergence of focused field studies of GH productivity, primarily within national GH programs (Moridis et al., 2009; 2010a). Together, these efforts have helped to clarify the dominant issues and challenges facing the extraction of methane from gas hydrates.

Classification of Gas Hydrate Deposits and Production Methods. Natural GH accumulations are divided into three main classes (Moridis and Collett, 2004) based on simple geologic features and the initial reservoir conditions. Class 1 settings are composed of two layers: a Hydrate-Bearing Layer (HBL) and an underlying two-phase fluid zone of mobile gas and liquid water. Because the base of the gas-hydrate stability zone (BGHSZ) coincides with the bottom of the HBL, this is the most desirable system as it is the easiest to destabilize and release gas (Moridis et al., 2008a; 2009). Class 2 settings comprise an HBL, overlying a zone of mobile water. Class 3 accumulations are composed of a single HBL, and are characterized by the absence of an underlying zone of mobile fluids. In Classes 2 and 3, the entire HBL may be at or well within the hydrate stability zone. A fourth class (Class 4) is typical of many oceanic accumulations, and involves disperse, low-saturation hydrate (<10%) deposits that lack confining geologic strata and are not targets for production (Moridis and Sloan, 2007).

Gas can be produced from GH by inducing dissociation by one of the following main methods (Makogon, 1997): (1) depressurization, in which the pressure P is lowered to a level lower than the hydration pressure P_e at the prevailing temperature T – see Figure 1, (2) thermal stimulation, in which T is raised above the hydration temperature T_e at the prevailing P, and (3) the use of inhibitors (such as salts and alcohols), which shifts the P_e-T_e equilibrium. Long-term production strategies often involve combinations of the three main dissociation methods (Moridis and Reagan, 2007a,b). Another production method involves CH_4 exchange with another hydrate-forming gas (e.g., CO_2) through a thermodynamically favorable reaction (White and McGrail, 2008; Graue et al., 2008).

Objectives. This investigation is part of an effort led by the U.S. Department of Energy to identify appropriate targets for a long-term field test of production from permafrost-associated hydrate deposits (Boswell et al, 2008). The main objectives of this study are:

(a) To evaluate the gas production potential of the C-Unit hydrate accumulation at the PBU L-106 site, North Slope, Alaska, during the planned long-term test
(b) To determine through sensitivity analysis the conditions and properties that affect the production performance, and which can serve as criteria to identify other deposits as suitable candidate for a successful field test of production if the hydrate deposit at the PBU L-106 site is deemed unsatisfactory,
(c) To determine the system response after the cessation of the long-term field test (i.e., after the well shut-in), and
(d) To compare the production performance from the C-Unit hydrate accumulation at the PBU L-106 site to that from the D-Unit deposit at the Mount Elbert site, North Slope, Alaska, which was the subject of an earlier study (Moridis et al., 2010b)

The PBU-L106 Site, North Slope, Alaska

Regional Geological System Description. The geology and petroleum geochemistry of the rocks on the North Slope of Alaska where gas hydrates are encountered are described in considerable detail in a number of publications (Bird and Magoon, 1987; Collett, 1993). The first direct confirmation of gas hydrate on the North Slope was provided by data from a single well (the Northwest Eileen State-2 well, located in the northwest part of the Prudhoe Bay Field), in which studies of pressurized core samples, downhole logs, and production testing had confirmed the occurrence of three gas-hydrate-bearing stratigraphic units (Collett, 1993).

Analysis of downhole log data from an additional 50 exploratory and production wells in the same area provided additional indications of hydrate occurrence in six laterally continuous sandstone and conglomerate units (A to F), which are all confined to the geographical area shown in Figures 2 and 3. Collett (2007) indicated that the hydrate units appear to trap down-dip several large free-gas accumulations (Figure 3; Units A through D). The volume of gas within the Eileen Gas Hydrate Accumulation (Collett, 2007) is estimated at about twice the volume of known conventional gas in the Prudhoe Bay Field (Collett, 1993), and ranges between 1.0×10^{12} and 1.2×10^{12} m^3 STP (Collett, 2007).

Previous Studies. Previous and current studies of gas production from hydrates in the North Slope of Alaska involve collaborations that are spearheaded by the BP Exploration (Alaska - BPXA), Inc., the U.S. Department of Energy, and the U.S. Geological Survey (USGS), and involve several other organizations. In 2003, the USGS initiated a study to develop seismic interpretive methods to identify and characterize GH accumulations in northern Alaska. This study dealt primarily with the analysis of a 3-D seismic data set from the area of the Milne Point Field as provided to the USGS by BP Exploration Alaska, Inc. (Figure 2). Detailed analysis and interpretation of available 3-D and 2-D seismic data sets, along with seismic modeling and correlation with specially processed downhole well log data, has led to the development of a viable method for identifying sub-permafrost GH prospects within the gas hydrate stability zone in the Milne Point area (Lee et al., 2010; Inks et al., 2010). This effort is supported by the Methane Hydrate Research and Development Act (enacted by the U.S. Congress in 2000 and renewed in 2005), and aims to determine the viability of the North Slope hydrates as an energy source (Mount Elbert Science Team, 2007) through investigations that will culminate with a long-term (1.5-2 years) field test of gas production (Boswell et al, 2008).

Analysis of geophysical surveys and well log data led the team to the installation of a well in 2007 at a previously undrilled, fault-bounded accumulation named the "Mount Elbert" prospect to acquire critical reservoir data needed to develop a longer-term production test program. The Mount Elbert-01 well was drilled to a depth of 915 m using chilled oil-based drilling fluid to avoid the inhibitor-induced dissociation caused by the salts and alcohols in conventional muds. A remarkable achievement was the recovery of significant lengths of core from the hydrate intervals, which were used for subsequent analyses of pore water geochemistry, microbiology, gas chemistry, petrophysical properties, and thermal and physical properties. After a battery of well log surveys was completed, a Schlumberger Modular Dynamic Testing (MDT) was conducted in two reservoir-quality sandy hydrate-bearing sections with high S_H (60% to 75%). Gas was produced from the gas hydrates in each of the tests. This study has yielded one of the most comprehensive datasets yet compiled on a naturally occurring gas hydrate geologic deposit (Collett, 2007).

Extensive discussions of the Mount Elbert geology and analyses of the various tests conducted at the site can be found in in Boswell et al. (2010).

The Unit C Hydrate Deposit at the PBU L-106 Site. The gas production performance of both the C- and D-Units at the Mount Elbert site (see Figure 2) during the proposed long-term test has been previously investigated (Anderson et al., 2008, Moridis et al., 2010b). Because of the relatively low temperature of these deposits due to their proximity to the permafrost (which lowers the amount of sensible heat available to fuel the endothermic dissociation process), the low pressure in these relatively shallow formations (which limit the maximum pressure drop attainable during the depressurization-induced hydrate dissociation and the corresponding gas production rate), and the extreme sensitivity of gas production to the hydrate temperature (Moridis and Reagan, 2007a,b; Moridis et al., 2010b), production from Units C and D at the Mount Elbert site was generally low. As a potentially more appealing alternative, the Prudoe Bay Unit (PBU) L-106 well site "downdip" from the Mount Elbert site (Figure 4) was investigated. The hydrate deposits at this site are deeper, more pressurized and warmer, and thus hold a promise of higher gas production.

Unit C extends from a depth of z = 678.5 m (2226 ft) to z = 723.6 m (2374 ft), and is composed of two hydrate-bearing strata: the deeper C1 and the shallower C2, 18.9 m (62 ft) and 17.1 m (56 ft) thick, respectively. These are that separated by a 9.2 m (30 ft) thick shale interlayer. This is a deposit bounded by impermeable shale top and bottom boundaries (Class 3), and is characterized by high intrinsic permeability (k = 1-5 Darcys), high porosity (ϕ = 0.4), high hydrate saturation (S_H = 0.75), a hydrostatic pressure P distribution varying between P_T = 7.3 and P_B = 7.7 MPa across the unit boundaries, and a temperature T ranging between T_T = 5 and T_B = 6.5 °C across the unit boundaries. In the absence of any samples or field data, the properties of the C-Unit (and its boundaries) at the PBU L-106 site are assumed to be the same as those of the C-Unit of the Mount Elbert site (Anderson et al., 2008), as they both belong to the same formation. These properties, as well as initial conditions such as pressure, temperature and saturations (which were unavailable at the site and were obtained from nearby wells), are listed in Table 1.

For reference, the single HBL of the D-Unit at the Mount Elbert site was thinner (11.3 m), had a T ranging between T_T = 2.3 ^oC and T_B = 2.6 ^oC at the HBL top and bottom, respectively, and P at the HBL top was a low P_T = 6.4 MPa (Moridis et al., 2010b). The temperature difference between the two units is very important: the study of Moridis et al. (2010b) has shown that a rise by 1 ^oC in the temperature of the D-Unit of the Mount Elbert deposit can lead to an eight-fold increase in the gas production rate.

The Numerical Models and Simulation Approach

The numerical simulation code. We used the TOUGH+HYDRATE simulator (Moridis et al., 2008b; Zhang et al., 2008) to conduct the numerical studies in this paper. This code (hereafter referred to as T+H) can model all the known processes involved in the system response of natural CH_4-hydrates in complex geologic media, including the flow of fluids and heat, the thermophysical properties of reservoir fluids, thermodynamic changes and phase behavior, and the non-isothermal chemical reaction of CH_4-hydrate formation and/or dissociation, which can be described by either an equilibrium or a kinetic model (Kim et al., 1998; Clarke and Bishnoi, 2001; Moridis and Kowalsky, 2008). T+H is a compositional simulator, and its formulation accounts for heat and up to four mass components (i.e., H_2O, CH_4, CH_4-hydrate, and water-soluble inhibitors such as salts or alcohols) that are partitioned among four possible phases: gas, aqueous liquid, ice, and hydrate. The T+H code can describe all the 15 possible thermodynamic states (phase combinations) of the CH_4+H_2O system and any combination of the three hydrate dissociation methods. It can handle the phase changes, state transitions, strong nonlinearities and steep solution surfaces that are typical of hydrate dissociation problems. Because of the very large computational requirements of this type of problem and the use of very large grids, we used the distributed-memory, massively parallel version of the code (Zhang et al., 2008) in the simulations discussed in this paper.

System geometry. The geologic system in this study corresponds to a location at the PBU L-106 site where the two HBLs (C1 and C2) and the shale interlayer have the thicknesses and dimensions discussed earlier. This is a complex variant of a Class 3 setting, in which the C2 and C1 HBLs are overlain and underlain, respectively) by nearly impermeable boundaries, i.e., shale strata. Based on experienced gained in earlier studies (Moridis and Reagan, 2007a;b; Moridis et al., 2008a) and preliminary scoping calculations, the simulation domain was extended 30 m into the overburden and underburden of the system, a distance that was deemed sufficient to allow accurate heat exchange with the deposit during the production period. The shale interlayer between C1 and C2 was assumed to be permeable, with a realistic $k = 5\text{x}10^{-15}$ m^2 (= 5 mD) and ϕ = 0.05.

We investigated the performance of both vertical and horizontal wells. The case of the vertical well, a single well was completed along the entire lengths of both the C1 and C2 HBLs. Because this is a long-term test and there is no information on outer boundaries, an infinite-acting system was assumed, and the outer radius of the cylindrical domain of the hydrate system was r_{max} = 2000 m.

Because of the lack of flow between C1 and C2 (caused by the shale interlayer), the horizontal well study involved two wells, one placed at the top of each one of the C1 and C2 HBLs HBL to capitalize on gas buoyancy and accumulation at this location, in addition to minimizing water production. In this case, the Cartesian domain was assumed to be rectangle in (x,y) with a length of 1000 m and a side of L_y = 1772.5 m. This corresponded to the same area as the domain in the cylindrical (single well) study, thus ensuring consistency by having the same surface area and hydrate volume in each simulation configuration. Both the vertical and the horizontal wells had a radius r_w = 0.1 m.

Domain discretization. For maximum accuracy, very fine grids were used in the simulation of production from both the cylindrical and rectangular sections of the hydrate deposit. The cylindrical domain of the single vertical well problem was discretized into 247x192 = 47,424 gridblocks in (r,z), resulting in a system of 189,696 equations. Discretization along the radial direction was non-uniform, increasing logarithmically from r_w to r_{max}, with Δr_0 = 0.05 m. Discretization along the z-axis was uniform (with Δz = 0.3 m) within the HBLs, the shale interlayer, and the boundaries in the immediate vicinity of the HBLs, but non-uniform (with Δz increasing) near the top and bottom of the domain. The Cartesian well of the horizontal well problem was discretized into 300x192 = 57,600 gridblocks in (r,z). Assuming an equilibrium reaction of hydrate dissociation during this long-term production process (Kowalsky and Moridis, 2007), and accounting for the water salinity, the grid resulted in a system of 230,400 equations.

In the study of the performance of the horizontal well, we used only a single slice of unit thickness on the (x,z) plane, i.e., perpendicular to the horizontal well. Implicit in this approach is the assumption of uniformity along the well length L_w, i.e., along the y-axis. While this assumption may not be always valid in light of expected pressure variations along the length of the well, it is a good first-order approximation, it can be used to bound the expected solution through the choice of an appropriate range of well pressures in the studied slices, and it allows high-definition in the description of the system behavior without resulting in a prohibitively large grid. As in the case of production from a single vertical well in a cylindrical section of the hydrate deposit, the 2D domain in (x,z) was discretized into 300x192 = 57,600 gridblocks, resulting in a system of 230,400 equations. The vertical discretization was the same as in the case of the cylindrical system. Discretization along x-axis was non-uniform, increasing logarithmically from $x_0 = r_w$ to L_x, with Δx_0 = 0.05 m.

Such a fine discretization is important (and possibly necessary) for accurate predictions when solid phases such as ice and hydrates are involved (Moridis et al., 2007). This high degree of refinement provided the level of detail needed to capture important processes near the wellbore and in the entire hydrate-bearing zone.

System properties and well description. As discussed earlier, the hydraulic and thermal properties of the various geological media (the HBL and the confining layers) in the C-Unit at the PBU L-106 site were assumed to be the same as in the C-Unit of Mount Elbert because of continuity of the same formation. These were obtained from data based on the first field test at the site (Anderson et al., 2008), and are listed in Table 1. We assumed that the initial hydrate and aqueous saturations (S_H and S_A, respectively) were uniformly distributed in the HBL, and that the overburden and underburden had both the same properties. The relative permeability relationships and the corresponding parameters were based on data obtained from history matching of the results of MDT test that had been conducted at the C-Unit at the Mount Elbert site (Anderson et al., 2008). The capillary pressure relationships and parameters were determined from the particle size analysis of porous media samples from C-Unit at the Mount Elbert site (White, 2008), and were consistent with the ϕ and k of the C-Unit at the PBU L-106 site.

Based on earlier studies that confirmed the validity of the approach (Moridis and Reagan, 2007b;c), we approximated wellbore flow by Darcian flow through a pseudo-porous medium describing the interior of the well. This pseudo-medium had $\phi = 1$, a very high $k = 10^{-9}$-10^{-8} m^2 (=1,000-10,000 Darcies), a capillary pressure $P_c = 0$, a relative permeability that was a linear function of the phase saturations in the wellbore, and a low (but nonzero) irreducible gas saturation $S_{irG} = 0.005$ (necessary to allow the emergence of a free gas phase in the well).

Initial and boundary conditions. The low effective permeability of the HBLs, the large system dimensions, and the relatively short production period resulted in an infinite-acting system in the simulations. We determined the initial conditions in the reservoir by following the initialization process described by Moridis and Reagan (2007a;b). In both the cylindrical and the rectangular systems, the uppermost and lowermost gridblock layers (i.e., at the top of the overburden and at the bottom of the underburden in the simulated domains, where Δz = 0.001 m) were treated as boundaries with constant conditions and properties. The temperatures at the upper and lower domain boundaries (T_U and T_L, respectively) were determined through a trial-and-error simulation process that resulted in the known T_P and T_B across the HBL. Note that the shales in the overburden and underburden were treated as impermeable (Table 1).

Knowing (a) the depth at the base of the HBL, and (b) assuming that the pressures in the subsurface follow the hydrostatic distribution—a hypothesis supported by earlier observations (Wright et al., 1999) in hydrate accumulations—we determined the pressure P_T (at z = 678.5 m) using the P-, T- and salinity-adjusted water density (1005 kg/m3 at atmospheric pressure). Then, using P_T and the boundary temperatures T_T and T_B, the hydrostatic gradient and representative thermal conductivity values were employed to determine the P- and T-profiles in the domains by means of a short simulation.

For reasons explained in detail by Moridis and Reagan (2007b), depressurization appears to be the most effective dissociation strategy, and a constant-pressure regime (involving a constant bottomhole pressure P_w at the well) is the most promising method of gas production from Class 3 hydrate deposits because of its simplicity, its technical and economic effectiveness, the fast response of hydrates to the rapidly propagating pressure wave, the near-incompressibility of water, and the large heat capacity of water. Because of the high initial hydrate saturation S_H in the HBL, the effective permeability k_{eff} is very low and constant-rate production is not feasible, while pure thermal stimulation is an unattractive option because of its limited effectiveness for reasons discussed in detail by Moridis and Reagan (2007a).

The numerical representation of a constant P_w involves treating the well as an internal boundary. In the case of a vertical well, this boundary is placed in the gridblock above the uppermost cell in the well. By imposing a constant P_w, a thermal conductivity k_Θ = 0 W/m/K, and a realistic (though unimportant) constant temperature T_w at this internal boundary, the correct constant bottohole-P condition was applied to the well while avoiding any non-physical temperature distributions in the well itself (the large advective flows into the uppermost gridblock from its immediate neighbor eliminated any unrealistic heat transfer effects that could have resulted from an incorrect k_Θ and/or T_w). In our study, the P_W = 3.0 MPa exceeds the pressure at the quadruple point PQ, thus eliminating the possibility of ice formation and the corresponding potentially adverse effect on k_{eff}.

Simulation process and outputs. The maximum simulation period was 2 years, i.e., the maximum expected duration of the long-term field test. In the course of the simulation, the following conditions and parameters were monitored: Spatial distributions of P, T, and gas and hydrate phase saturations (S_G and S_H); Volumetric rates of CH_4 released from dissociation and of CH_4 production at the well (Q_R and Q_P, respectively); Cumulative volumes of CH_4 released from dissociation, produced at the well, or remaining in the deposit as free gas (V_R, V_P and V_F, respectively); Water mass production rate at the well (Q_W) and cumulative mass of produced water (M_W).

Production Using a Vertical Well

Gas production and water production. Figure 6 shows the evolution of Q_R and Q_P from the single vertical well at the center of the cylindrical reservoir over time. The most important conclusions from the review of Figure 6 is that (a) the Q_R and Q_P increase monotonically, (b) they are very close in value, with Q_R being slightly higher than Q_P, and (c) Q_R and Q_P remain relatively low for the entire 2 years of the production period. Thus, at no time Q_R and Q_P exceed 2,500 ST m^3/day (89,000 ST ft^3/day) during the 2 yers of the test. The low production rate is caused by the relatively low initial temperature of the hydrate in the HBLs. The low T reduces the rate of the dissociation reaction and severely reduces the sensible heat that is available to support it.

The cumulative produced volume V_P in Figure 7 provides further confirmation of the limited productivity of the C-Unit at the PBU L-106 site as a target for production from hydrates by depressurization using a vertical well: after continuous production for t = 2 years, $V_P < 8\text{x}10^5$ ST m^3 (=$2.8\text{x}10^7$ ST ft3) of CH4 have been produced. $V_P < V_R$ during the entire production period (Figure 7). Note the very low level of free gas, V_F, in the reservoir during production (Figure 7), which exhibits a very mild upward trend during the 2 years of the test. The low levels of V_F, and the near-parity of V_R and V_P (and Q_R and Q_P), indicate that there is little gas accumulation in the reservoir, and most of the gas released from dissociation and dissolution is produced at the vertical well.

The water production rate Q_W in Figure 8 reaches high level for a very short time at the beginning of production (when the pressure drop $\Delta P = P_0 - P_W$ is at a maximum), then drops as the low k_{eff} of the HBLs does not allow large water flows, and thne begins to increase continuously as the hydrate dissociates and k_{eff} increases. The most important observation from Figure 8 is that Q_W and M_W remain at easily manageable levels.

Property distributions. The evolution of P-distribution over time in Figure 9 is consistent with expectations. Pressure drops along the two production intervals, i.e., the entire thicknesses of the two HBLs. The permeable shale interlayer has initially higher permeability than the HBLs, resulting in a larger pressure drop there. As time advances, the area of depressurization increases. However, at t = 730 days, it is easy to see from the last picture that only a fraction of the 2,000 reservoir radius is exhibiting depressurization, indicating that the system is indeed infinite-acting.

The evolution of T-distribution over time in Figure 10 shows a slowly (but consistently) expanding area of lower temperatures, denoting the expanding dissociation zone and the consequent cooling caused by the endothermic nature of the reaction. The evolutions S_H and S_G distributions in Figures 11 and 12, respectively, confirm the observations from Figures 6 and 7: hydrate dissociation appears to have barely affected the main body of the hydrate at the end of the 2-year production test, with signs of dissociation limited to a narrow zone around the production intervals and at the bounding planes of the 2 HBLs.

The low free gas volume V_F seen in Figure 7 is consistent with the observations from Figure 12, which shows very limited gas accumulation in the reservoir. Most of the gas is found along bottom of the C1 stratum and the top of the C2 layer, confirming the evolution of the upper dissociation interface that is the hallmark of all depressurization-induced dissociation behavior.

Sensitivity Analysis

We investigated the sensitivity of gas production to the following conditions and parameters:

(a) The initial hydrate saturation S_H
(b) The intrinsic permeability k
(c) The permeability of the shale boundaries k_B
(d) The type of the well (vertical vs. horizontal).

Sensitivity to S_H. Figure 13(a) shows that Q_R and Q_P increases with a decreasing S_H, at least within the range we investigated ($0.50 \leq S_H \leq 0.75$). This is attributed to the higher k_{eff} that corresponds to lower S_H levels for a given intrinsic permeability k. However, the effect of S_H is a function of time. It can be seen that this behavior is not consistent: it holds true for times early in the production process, but it is completely reversed at later time. Thus, at t = 500 days, Q_R and Q_P increases with an increasing S_H, but at t = 720 days, Q_P for $S_H = 0.50$ and $S_H = 0.65$ are practically the same, and the trend is for Q_P for $S_H = 0.50$ to be higher than that for $S_H = 0.65$. It is not known if this will be a persistent behavior or the result of temporary fluctuations. Note that the gap between Q_R and Q_P (with $Q_R < Q_P$) increases with a decreasing S_H, indicating an increasing contribution of dissolved gas to toatal production; for $S_H = 0.75$, $Q_P < Q_R$.

The evolution of the cumulative volumes V_R and V_P in Figure 13(b) reflects the relative sizes of Q_R and Q_P. Thus, V_R and V_P initially increase with a decreasing S_H, but the trend is reversed at later times. The levels of V_F are very low, indicating limited gas accumulation in the reservoir.

In Figure 14, the water production rates Q_w and cumulative mass of produced water M_w associated with depressurization-induced gas production from the hydrates at the PBU L-106 site show a clear pattern, increasing with a decreasing S_H. They differ very substantially for the various S_H in the study because they reflect drastically different k_{eff} regimes (strongly influenced by S_H). Q_w decreases over time because the driving force ΔP in the reservoir decreases as depressurization advances, and eventually the three Q_w appear to stabilize (at least within the time frame of this study – it is unlikely that this pattern will persist at later times).

Sensitivity to the formation intrinsic permeability k. Figure 15 shows that V_R and V_P both increase with an increasing k, (as do the corresponding Q_R and Q_P). This was expected because a higher k leads to a higher k_{eff}. Similarly, the water production rates Q_w and the cumulative mass of produced water M_w in Figure 16 increase with an increasing k, and follow the same pattern identified in the reference case of Figure 8.

Sensitivity to the intrinsic permeability of the shale boundaries k_B. Figure 17 shows that both Q_R and Q_P decrease rapidly with an increasing k_B because of the reduced effectiveness of depressurization (as the permeable boundaries admit fluids and do not allow a sufficiently strong pressure drop). An increasing k_B leads to an imbalance in the magnitudes of Q_R and Q_P. From rough parity for $k_B = 0$, Q_P becomes larger than Q_R, with increasing amounts of gas contributed from dissolved gas. Additionally, because of the increased permeability of the boundary, water production increses drastically (Figure 18).

Production Using a Horizontal Well

Gas production. Figure 19 shows the evolution of Q_R and Q_P from a horizontal well over time, and includes for reference the Q_R and Q_P corresponding to the vertical well (from Figure 6). The use of the horizontal well is shown to increase both Q_R and Q_P by a minimum of a factor of 4 (and by well over an order of magnitude early in the production period). While the improvement in performance over the vertical well is dramatic, Q_P remains moderate in absolute terms. However, it is possible that the production outlook may improve with longer wells, different well configurations, more complex production strategies, and by the consideration of heterogeneity (which has been shown to improve production in layered systems such as the ones in Units C and D of Mount Elbert – see Kurihara et al., 2005; 2009).

The evolution of Q_R and Q_P is characterized by an initial period (Stage 1, to t = 300 days) of linear increase, and is succeeded by a period of relative stability (stage 2) that lasts until the end of the long-term test at t = 720 days. At the end of Stage 1, $Q_P = 9\text{x}10^3$ ST m^3/day (= $3.2\text{x}10^5$ ST ft^3/day), and in Stage 2 it stabilizes at this level.

Stage 1 is associated with rapid depressurization (especially near the wellbore) and corresponds to the rapid advancement of the depressurization front in the deposit. Because (a) the pressure drop $\Delta P = P_0 - P_w$ between the bottomhole pressure and the pressure at the dissociation front is at its maximum ΔP_{max} in the HBL, and (b) dissociation expands continuously into unaffected parts of the HBL as the depressurization front advances quickly, Q_R and Q_P increase rapidly and dQ_R/dt and dQ_R/dt are at their maximum. The endothermic nature of the hydrate dissociation reaction results in cooling of the HBL, but this has a limited effect in countering the effects of ΔP on subsequent dissociation.

The end of Stage 1 and onset of Stage 2 is marked by the depressurization front reaching the outer boundaries of the HBL domain (i.e., at $y = L_y$, $x = L_x$). When this happens, the pressure wave can no longer advance, and the pressure drop at any point in the domain $\Delta P = P - P_w < \Delta P_{max}$. While Q_R and Q_P continue to increase because a larger volume of hydrate is dissociating, they do so slower, i.e., the lower pressure gradient leads to the reduction in dQR/dt and dQP/dt, which remain positive. Additionally, continuing HBL cooling caused by advancing hydrate dissociation makes further dissociation progressively more difficult.

Finally, the continuously diminishing driving force of dissociation (i.e., the ΔP) and the parallel reduction in the sensible heat that fuels and supports it eventually lead to a decline Q_R and Q_P. However, we do not observe it in our study because of the relatively short duration of the test and the low Q_R and Q_P, which do not materially affect the bulfk of the hydrate mass in the 2-year time frame.

Q_R and Q_P in Figure 19(a) are very similar in magnitude, as was the case in production from a vertical well. Similar to the reference case of the vertical well problem, $Q_R > Q_P$ during production from the horizontal well. We observe a similar pattern in the relationship of V_R and V_P in Figure 19(b), with V_R being very slightly larger than V_P, while both (and V_F) are several

times larger larger than the ones corresponding to the vertical well case. Review of the relative magnitudes of Q_R, Q_P, V_R, V_P, and V_F confirms the pattern identified in the vertical well case, i.e., little gas accumulation in the reservoir, with most of the gas released from dissociation and dissolution is produced at the horizontal well. The cumulative produced volume V_P in Figure 19(b) provides further confirmation of the improved outlook, which, while not being spectaccular, is respectable for onshore production.

Water production. The water production rate Q_W in Figure 20 exhibits fluctuations, but, after an initial phase of declining Q_W, appears on average to be roughly stable as it oscillates about a relatively stable mean. This is confirmed by the near-linear pattern of the M_W graph in Figure 20. A declining long-term trend is (a) an inevitable consequence of a continuously declining pressure differential ΔP, and (b) consistent with observations and conclusions from previous studies of production from hydrates (Moridis et al, 2007a;b; Moridis et al., 2010b), but the short duration of the test and the small fraction of the hydrate mass that has been destroyed during it do not allow us to observe this decline. While M_W is larger (as expected) in the horizontal well case, it remains at manageable levels.

System Response During A Well Shut-In

An important question that needs to be answered as the long-term field is planned is the response of the hydrate deposit upon the cessation of production because this will define the time frame of the study, and will address persitent worries that continuing dissociation after the well shut-in may cause complications. Figure 21 shows the evolution of Q_R (describing the net rate of hydrare dissociation in the entire deposit after a well shut in. The rates of CH_4 release Q_R decrease initially. Q_R is initially positive (indicating continuing dissociation because of pressure gradients in the deposit after the well shut-in), but then becomes negative (indicating hydrate formation near the well as P increases). After a short time (the duration of which is closely related to the exhaustion of free gas in the deposit), Q_R drops rapidly to near-zero levels, indicating disappearance of free gas and cessation of hydrate formation or dissociation at t = 80 – 110 days past the well shut in. Past that point, some low-level activity (indicated by $Q_R > 0$) continues for a long time, and denotes long-term hydrate dissolution and redistribution as heat from the boundaries continues to flow into the deposit and a pressure and geothermal equilibrium are re-established.

The cumulative volume of released CH_4 (V_R) after the well shut-in in Figure 22 is positive in all cases, indicating continuing net hydrate dissociation. This is caused by residual pressure gradients that persist within the deposit, and which allow continuing dissociation away from the well. These pressure differentials decline rapidly, leading to higher pressures in the vicinity of the well (where T is low), secondary hydrate formation and rapidly declining V_R. This results in the negative V_R) values that are observed after a short time (<10 days) following the well shut-in, which denote hydrate formation.

Comparison to the Production Performance of Unit D at the Mount Elbert Site, North Slope, Alaska

Figure 23 shows the production and release rates Q_R and Q_P for the D-Unit at the Mount Elbert site (Moridis et al., 2010b) using both horizontal and vertical wells. If the magnitude of the rate of gas production is the absolute criterion for success of the proposed field test, then the superiority of the C-Unit at the PBU L-106 site is evident: the corresponding Q_R in Figure is 19 is several times higher than that for the D-Unit at the Mount Elbert site. There are two reasons for this superior production performance. The first is the higher formation temperature, which is known to be probably the most important factor affecting production (all other issues being equal). The second reason is the considerably larger thickness of the HBLs at the PBU L-106 site, resulting in a larger gas source.

Summary and Conclusions

This study is part of an effort led by the U.S. Department of Energy to identify appropriate targets for a long-term field test of production from permafrost-associated hydrate deposits. We focus on the evaluation of the gas production potential of a gas hydrate deposit in the C-Unit of the PBU L-106 site on the North Slope, Alaska. We investigate the performance of vertical and horizontal wells operating under constant bottomhole pressure in gas production fueled by depressurization-induced dissociation of the hydrates. Based on the results of this study, we draw the following conclusions:

(1) Preliminary calculations indicate that a long-term test of gas production from a gas hydrate deposit (Unit C) at the PBU-L106 site using a single vertical well is feasible. The production rate Q_P is predicted to increase consistently during the duration of the long-term test (up to 2 years). However, Q_P is generally low be cause of relatively low temperatures (5 to 6.5 °C) and pressure (limiting the magnitude and effectiveness of depressurization), with a maximum Q_P = 2,250 ST m^3/day (about 80 MSCFPD), and a cumulative volume of produced gas V_P = 80,000 ST m^3 (about 2.81 MMSCF).

(2) The water production rates Q_W, and the corresponding cumulative mass of produced water Q_W, are modest and can be easily handled during production.

(3) Q_W and M_W increase with an increasing intrinsic permeability k, and with a decreasing permeability of the shale boundaries (overburden and underburden) k_B of the hydrate deposit.

(4) The effect of the initial hydrate saturation S_{H0} on Q_P and V_P is not monotonic or straightforward, and is a function of time; initially, Q_P and V_P increase with a decreasing S_{H0} because of a higher effective permeability (and, thus, easier dissociation), but the effect is reversed at later times.

(5) The use of horizontal wells can increase Q_P and V_P by orders of magnitude (with a V_P reaching 5.27×10^6 ST m^3 = 186 MMSCF at the end of the production test for a well of length L = 1000 m). The corresponding increase in water production remains well within manageable limits.

Acknowledgment

This work was supported by the Assistant Secretary for Fossil Energy, Office of Natural Gas and Petroleum Technology, through the National Energy Technology Laboratory, under the U.S. Department of Energy, Contract No. DE-AC02-05CH11231. The authors are indebted to John Apps and Dan Hawkes for their careful review.

References

Anderson, B.J., Wilder, J.W., Kurihara, M., White, M.D., Moridis, G.J., Wilson, S.J., Pooladi-Darvish, M., Masuda, Y., Collett, T.S., Hunter, R.B., Narita, H., Rose, K. and Boswell, R., 2008. Analysis of Modular Dynamic Formation Test Results From the Mount Elbert-01 Stratigraphic Test Well, Milne Point Unit, North Slope, Alaska**,** paper presented at the 6th International Conference on Gas Hydrates, Vancouver, British Columbia, Canada, July 6-10, 2008.

Bird, K.J., and Magoon, L.B., 1987, Petroleum geology of the northern part of the Arctic National Wildlife Refuge, Northeastern Alaska: *U.S. Geological Survey Bulletin* **1778**, 324.

Boswell, R., Hunter, R., Collett, T.S., Digert, S., Hancock, M., Weeks, M. 2008. Investigation of gas hydrate bearing sandstone reservoir at the Mount Elbert stratigraphic test well, Milne Point, Alaska. *Proc.* 6th International Conference on Gas Hydrates, July 6 – 10, 2008, Vancouver, BC.

Boswell, R., Collett, T., Anderson, B., Hunter, R., eds., 2010, Scientific results of the BPXA-USDOE-USGS Mount Elbert gas hydrate stratigraphic test well, Milne Point Unit, Alaska North Slope. *J. Marine Pet. Geo.*

Clarke, M.A., and Bishnoi, P.R., 2000. Determination of the Intrinsic Rate of Methane Gas Hydrate Decomposition", *Chem. Eng. Sci.*, **55**, 4869.

Collett, T., 1993, Natural gas hydrates of the Prudhoe Bay and Kuparuk River area, North Slope, Alaska: American Association of Petroleum Geologists Bulletin, **77** (5), 793-812.

Collett, T., 1995. *1995 National Assessment of U.S. Oil and Gas Resources* (on CD-ROM) (Gautier, D.L., Goldton, G.L. et al., eds.), USGS.

Collett, T., 2007. Arctic Gas Hydrate Energy Assessment Studies, The Arctic Energy Summit, ANCHORAGE, ALASKA • 15-18 OCTOBER 2007

Dallimore, S.R., Uchida, T., and Collett, T.S., 1999, Scientific results from JAPEX/JNOC/GSC Mallik 2L-38 gas hydrate research well, Mackenzie Delta, Northwest Territories, Canada, *Geological Survey of Canada Bulletin* **544**, 403.

Dallimore, S.R., and Collett, T.S., Eds., 2005. Scientific Results from the Mallik 2002 Gas Hydrate Production Research Well Program, Mackenzie Delta, Northwest Territories, Canada, *Geological Survey of Canada Bulletin* **585**.

Graue, S., Kvamme, B., Baldwin, B.A., Stevens, J., Howard, J., Aspenes, E., Ersland, G., Husebo, J., Zomes, D., M. 2008. MRI Visualization of Spontaneous Methane Production From Hydrates in Sandstone Core Plugs When Exposed to CO2. *SPE J.* 13(2): 146-152, (doi: 10.2118/118851-PA).

Inks, T.L., Lee, M.W., Agena, W.F., Taylor, D.J., Collett, T.S., Hunter, R.B., Zyrianova, M.V., 2010. Seismic prospecting for gas hydrate and associated free-gas prospects in the Milne Point area of northern Alaska, in Collett, T., Johnson, A., Knapp, C., Boswell, R., eds, Natural Gas Hydrates -- Energy Resource Potential and Associated Geologic Hazards: *American Association of Petroleum Geologists Memoir* **89**.

Kim, H.C., Bishnoi, P.R., Heidemann, R.A., and Rizvi, S.S.H., 1987. Kinetics of Methane Hydrate Decomposition, *Chem. Eng. Sci*., **42**(7), 1645.

Klauda, J.B., and Sandler, S.I., 2005. Global distribution of methane hydrate in ocean sediment, *Energy & Fuels* **19**, 469.

Kowalsky, M. B., and Moridis, G.J., 2007, Comparison of kinetic and equilibrium reactions in simulating the behavior of gas hydrates, *Energy Conversion and Management*, **48**, 1850, doi:10.1016/j.enconman.2007.01.017 (LBNL-63357).

Kurihara, M., Funatsu, K., Ouchi, H., Masuda Y. and Narita, H., 2005b. Investigation On Applicability Of Methane Hydrate Production Methods To Reservoirs With Diverse Characteristics, Paper 3003 presented at the 5th International Conference on Gas Hydrates, Trondheim, Norway, 13–16 June, Proceedings, Vol. 3, 714-725.

Kurihara, M., Sato, A., Ouchi, H., Narita, H., Masuda, Y., Saeki, T., and Fujii, T. 2009. Prediction of Gas Productivity from Eastern Nankai Trough Methane-Hydrate Reservoirs. *SPE Res Eval & Eng* **12** (3): 477-499. SPE-125481-PA. doi: 10.2118/125481-PA.

Kvenvolden, K.A., 1988. Methane hydrate--A major reservoir of carbon in the shallow geosphere? *Chem. Geo*. **71**: 41-51.

Lee, M.W., Collett, T.S., Inks, T.L., 2010. Seismic attribute analysis for gas-hydrate and free-gas prospects on the North Slope of Alaska, in Collett, T., Johnson, A., Knapp, C., Boswell, R., eds, Natural Gas Hydrates -- Energy Resource Potential and Associated Geologic Hazards: *American Association of Petroleum Geologists Memoir* **89**.

Milkov, A. V., 2004. Global estimates of hydrate-bound gas in marine sediments: How much is really out there? *Earth Science Reviews* **66** (3), 183.

Makogon, Y.F., 1987. Gas hydrates: frozen energy, *Recherche* **18** (192), 1192.

Makogon, Y.F., 1997. *Hydrates of Hydrocarbons*. Penn Well Publishing Co. Tulsa, OK.

Moridis, G.J., 2003. Numerical Studies of Gas Production From Methane Hydrates, *SPE Journal*, **32**(8), 359.

Moridis, G.J., Collett, T.S. 2004. Strategies for Gas Production from Hydrate Accumulations Under Various Geologic Conditions, LBNL-52568, Lawrence Berkeley National Laboratory, Berkeley, CA.

Moridis, G.J., and Sloan, E.D., 2007. Gas Production Potential of Disperse Low-Saturation Hydrate Accumulations in Oceanic Sediments, *J. Energy Conversion and Management*, **48** (6), 1834-1849.

Moridis, G.J., Collett, T., Dallimore, S., Satoh, T., Hancock, S., and Weatherhill, B., 2004. Numerical Studies Of Gas Production From Several Methane Hydrate Zones At The Mallik Site, Mackenzie Delta, Canada, *JPSE* **43**, 219.

Moridis, G.J., and Reagan, M.T., 2007a. Strategies for Gas Production From Oceanic Class 3 Hydrate Accumulations, *OTC-18865*, 2007 Offshore Technology Conference, Houston, Texas, 30 April – 3 May 2007.

Moridis, G.J., and Reagan, M.T., 2007b. Gas Production From Oceanic Class 2 Hydrate Accumulations, *OTC 18866*, 2007 Offshore Technology Conference, Houston, Texas, U.S.A., 30 April–3 May 2007.

Moridis, G.J., and Reagan, M.T., 2007c. Gas Production From Class 2 Hydrate Accumulations in the Permafrost, *SPE 110858*, 2007 SPE Annual Technical Conference and Exhibition, Anaheim, California, U.S.A., 11–14 November 2007.

Moridis, G.J., Sloan, E.D. 2007. Gas Production of disperse low-saturation hydrate accumulations in oceanic sediments. *Energy Conversion and Management* **48**: 1834-1849.

Moridis, G.J., Kowalsky, M., and Pruess, K., 2008a. Depressurization-Induced Gas Production From Class 1 Hydrate Deposits, *SPE Reservoir Evaluation and Engineering*, **10** (5), 458-488.

Moridis, G.J., Kowalsky, M.B., and Pruess, K., 2008b. TOUGH+HYDRATE v1.0 User's Manual: A Code for the Simulation of System Behavior in Hydrate-Bearing Geologic Media, Report LBNL-00149E, Lawrence Berkeley National Laboratory, Berkeley, CA.

Moridis, G.J., Collett, T.S., Boswell, R., Kurihara, M., Reagan, M.T., Sloan, E.D., Koh, C., 2009. Toward production from gas hydrates: assessment of resources and technology and the role of numerical simulation. *SPE Reservoir Evaluation & Engineering*, 12(5): 745-771 (doi: 10.2118/114163-PA).

Moridis, G.J., T.S. Collett, M. Pooladi-Darvish, S. Hancock, C. Santamarina, R. Boswell, T. Kneafsey, J. Rutqvist, M. Kowalsky, M.T. Reagan, E.D. Sloan, A.K. Sum and C. Koh, 2010a. Challenges, Uncertainties and Issues Facing Gas Production From Hydrate Deposits in Geologic Systems, Invited Paper SPE 131792, 2010 Unconventional Gas Conference, February 23-25, Pittsburgh, PA.

Moridis, G.J., S. Silpngarmlert, M.T. Reagan, T.S. Collett, and K. Zhang, 2010b. Gas Production From a Cold, Stratigraphically Bounded Hydrate Deposit at the Mount Elbert Site, North Slope, Alaska, In press, *Journal of Marine and Petroleum Geology*, 2010 (doi: 10.1016/j.marpetgeo.2010.01.005, LBNL-3005E).

Reagan, M.T., Moridis, G.J., and Zhang, K., 2008. Sensitivity Analysis of Gas Production from Class 2 and Class 3 Hydrate Deposits, OTC 19554, 2008 Offshore Technology Conference, Houston, Texas, USA, 5-8 May 2008.

Sloan, E.D., and Koh, C., 2008. *Clathrate Hydrates of Nautral Gases.* 3rd Edition, Taylor and Francis, Inc., Boca Raton, FL.

Sun, X., and Mohanty, K.K., 2005. Simulation of Methane Hydrate Reservoirs, SPE 93015, 2005 SPE Reservoir Simulation Symposium, Houston, TX U.S.A., 31 January - 2 February 2005.

van Genuchten, M.Th., 1980. A Closed-Form Equation for Predicting the Hydraulic Conductivity of Unsaturated Soils", *Soil Sci. Soc.*, **44**, 892.

White, M., 2008. Personal communication.

White, M., McGrail, B.P, 2008. Numerical Simulation of Methane Hydrate Production from Geologic Formations via Carbon Dioxide Injection, Paper OTC-19458-MS, Offshore Technology Conference, 5-8 May 2008, Houston, Texas, USA (doi: 10.4043/19458-MS).

Wright, J.F., Dallimore, S.R., and Nixon, F.M., 1999. Influences of Grain Size and Salinity on Pressure-Temperature Thresholds for Methane Hydrate Stability in JAPEX/JNOC/GSC Mallik 2L-38 Gas Hydrate Research-Well Sediments, in Scientific Results from JAPEX/JNOC/GSC Mallik 2L-38 Gas Hydrate Research-Well, Mackenzie Delta, Northwest Territories, Canada. Dallimore, S.R., Uchida, T., and Collett, T.S., Eds., *Geological Survey of Canada Bulletin* **544**, 229.

Zhang, K., and Moridis, G.J., 2008. A Domain Decomposition Approach for Large-Scale Simulations of Coupled Processes in Hydrate-Bearing Geologic Media**,** paper presented at the 6th International Conference on Gas Hydrates, Vancouver, British Columbia, Canada, July 6-10, 2008.

Table 1 – Hydrate Deposit Properties used in the study of Unit C, PBU L-106 (Taken from the C-Unit of Mount Elbert and nearby wells)

Parameter	Value
C1 Hydrate zone thickness	18.9 m
C2 Hydrate zone thickness	17.1 m
Shale interlayer tickness	9.2 m
Initial pressure at top of HBL (P_T)	7.3 MPa
Initial temperature at top of HBL (T_T)	5.0 ^oC
Initial temperature at base of HBL (T_B)	6.3 ^oC
Gas composition	100% CH_4
Initial saturations in the HBL	S_H = 0.75, S_A = 0.25
Intrinsic permeability of HBL $k_r = k_x = k_z$	10^{-12} m^2 (= 1 D)
Porosity of HBL ϕ	0.4
Compressibility of HBL	$5x10^{-9}$ Pa^{-1}
Intrinsic permeability $k_r = k_x = k_z$ (overburden & underburden)	0 m^2 (= 0 D)
Porosity of overburden & underburden	0.005
Grain density ρ_R (all formations)	2750 kg/m^3
Constant bottomhole pressure (P_w)	3 MPa
Dry thermal conductivity ($k_{\Theta RD}$) (all formations)	0.5 W/m/K
Wet thermal conductivity ($k_{\Theta RW}$) (all formations)	3.1 W/m/K
Composite thermal conductivity model (Moridis et al., 2008c)	$k_{\Theta C} = k_{\Theta RD} + (S_A^{1/2} + S_H^{1/2})\,(k_{\Theta RW} - k_{\Theta RD}) + \phi\, S_I\, k_{\Theta I}$
Capillary pressure model (vanGenuchten, 1980)	$P_{cap} = -P_0 \left[\left(S^* \right)^{-1/\lambda} - 1 \right]^{\lambda}$ $S^* = \frac{(S_A - S_{irA})}{(S_{mxA} - S_{irA})}$
S_{irA}	1
λ (White, 2008)	0.77437
P_0 (White, 2008)	$5x10^3$ Pa
Relative permeability model (Moridis et al., 2008b)	$k_{rA} = (S_A^*)^n$ $k_{rG} = (S_G^*)^m$ $S_A^* = (S_A - S_{irA})/(1 - S_{irA})$ $S_G^* = (S_G - S_{irG})/(1 - S_{irA})$ EPM model
n; m (from Anderson et al., 2008)	4.2; 2.5
S_{irG}	0.02
S_{irA}	0.20

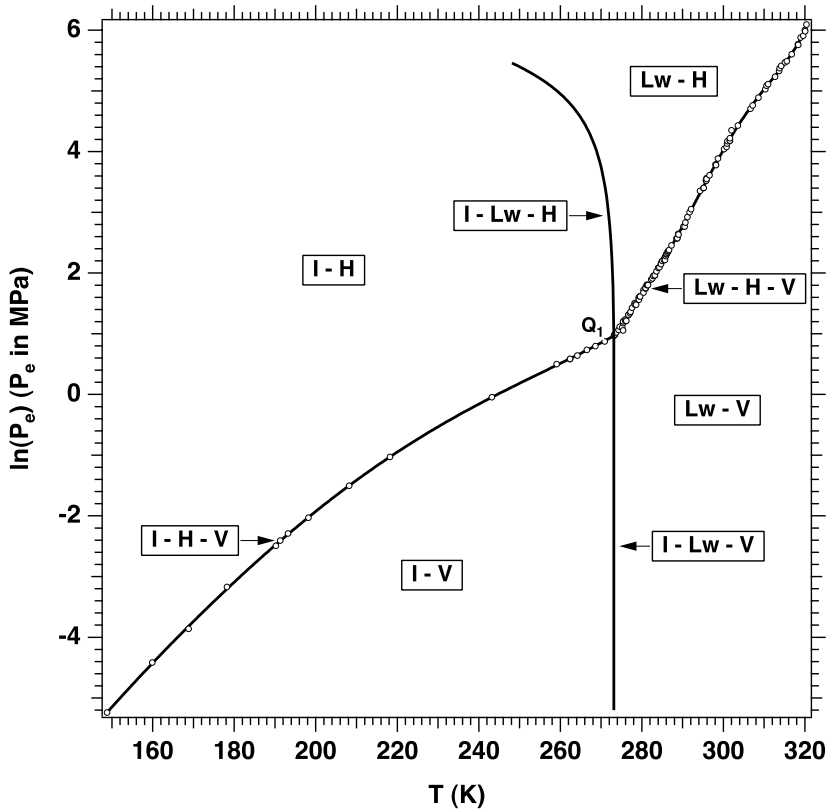

Figure 1. Pressure-temperature equilibrium relationship in the phase diagram of the water–CH_4–hydrate system (Moridis, 2003), Lw: Liquid water; H: Hydrate; V: Vapor (gas phase); I: Ice; Q_1: Quadruple point = I + Lw + H + V). The two arrows show the direction of increasing thermodynamic desirability of a deposit as a production target.

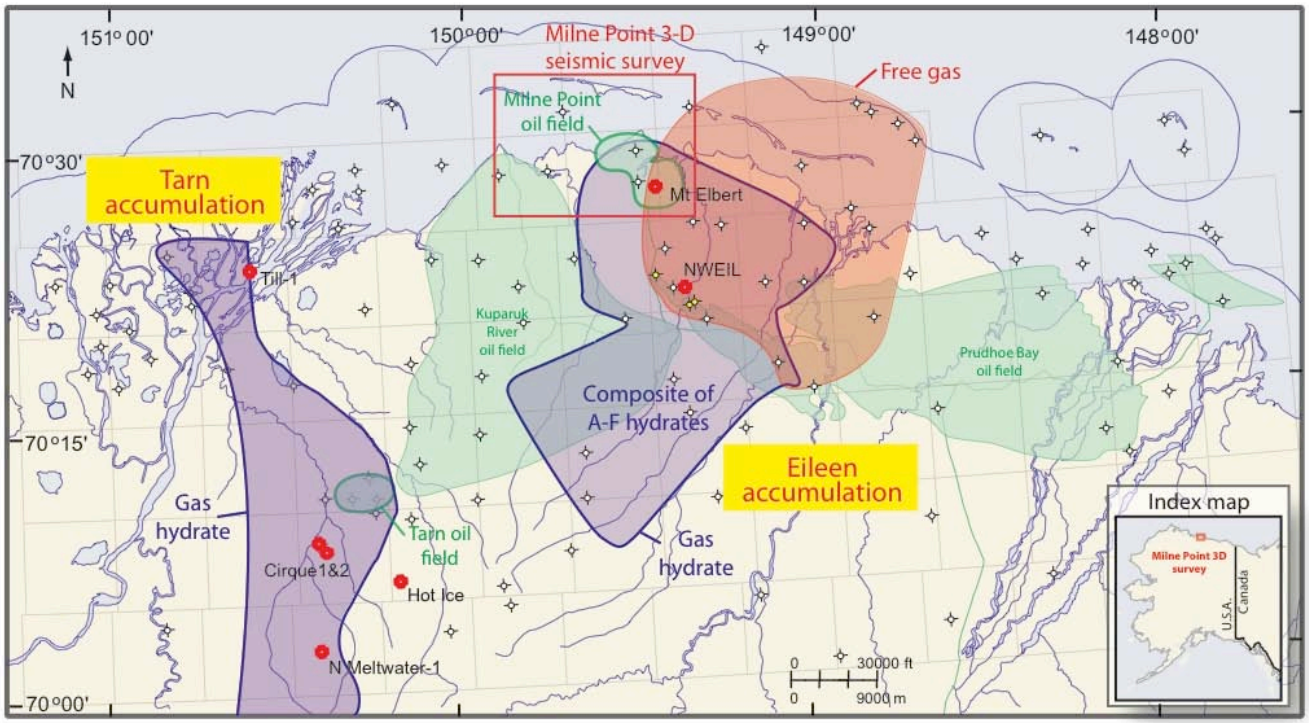

Figure 2 - Map of the Eileen and Tarn gas hydrate accumulations overlying portions of the Prudhoe Bay, Kuparuk River, and Milne Point oil fields (modified from Collett, 1993). The locations of the Northwest Eileen State-2 (NWEIL) and Mount Elbert gas hydrate research wells are shown, along with the outline of the Milne Point 3D seismic volume used to identify and map gas hydrate prospects.

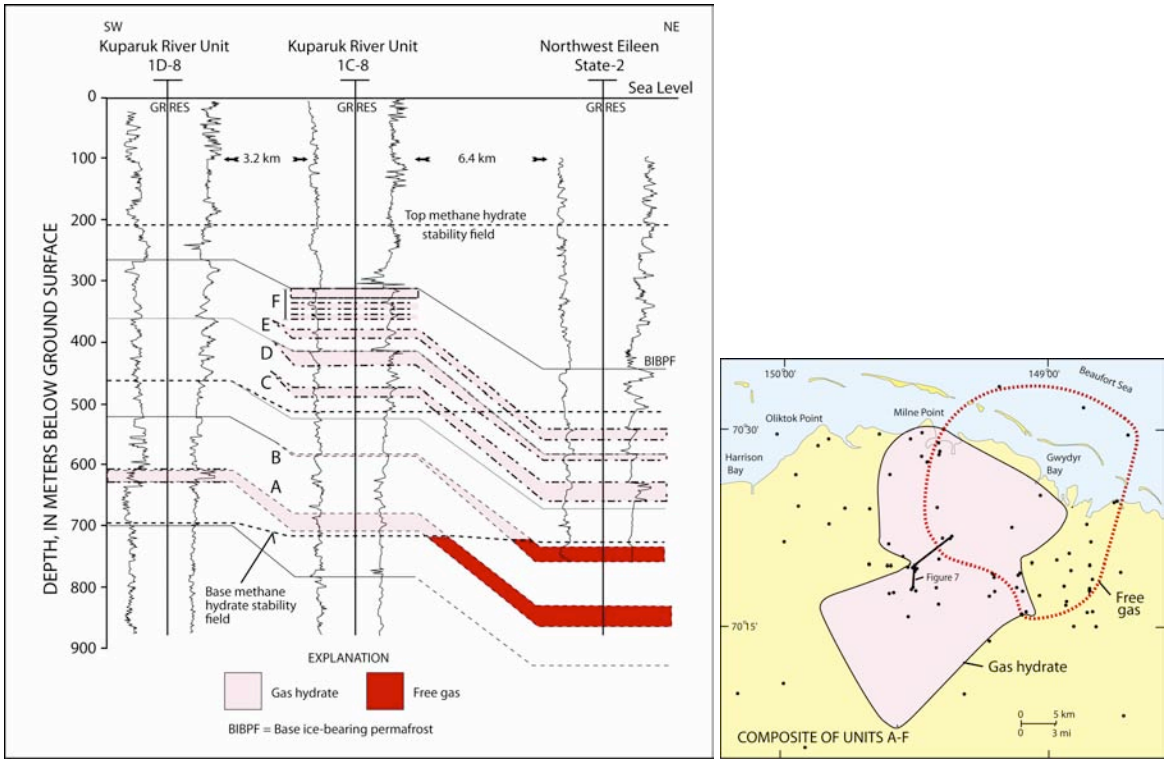

Figure 3. (a) Cross section showing the lateral and vertical extent of gas hydrates and underlying free-gas occurrences in the Prudhoe Bay-Kuparuk River area in northern Alaska. See Figure 3(b) for location of cross section. The gas-hydrate-bearing units are identified with the reference letters A through F (Collett, 1993), and their positions relative to the permafrost and to the base of the hydrate stability zone are shown; (b) Composite map of all six gas-hydrate/free-gas units (Units A-F) from the Prudhoe Bay-Kuparuk River area in northern Alaska (Collett, 1993).

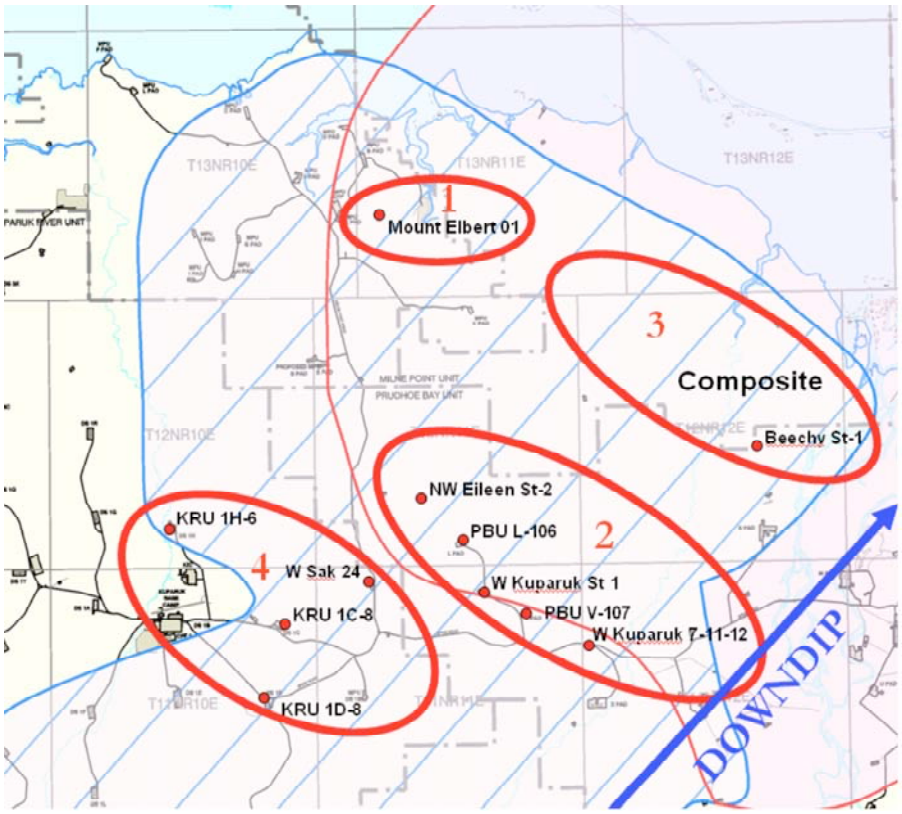

Figure 4: Map of composite lateral extent of Sagavanirktok gas hydrate bearing zones A, B, C, D, E, and F (blue with stripes) showing the relative locations of the Mount Elbert and PBU L-106 sites.

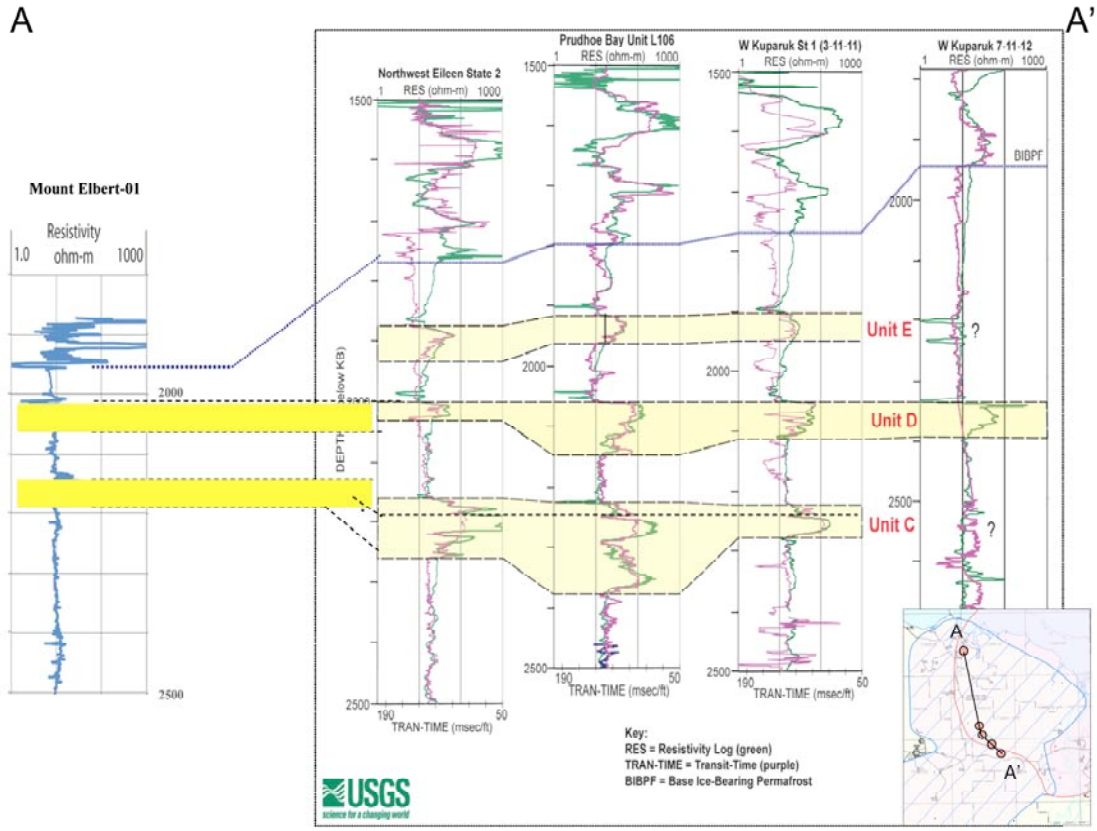

Figure 5: Cross section "downdip" from Mount Elbert across Area 2 (see Figure 4), through the PBU L-106 well.

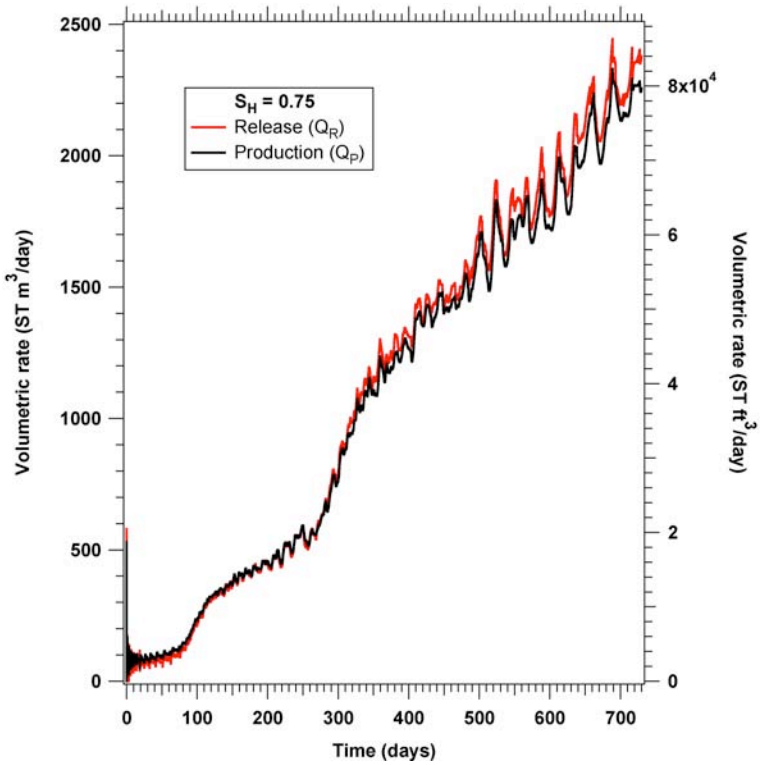

Figure 6 - Q_R and Q_P during a proposed long-term production test from the hydrate deposits in the C-Unit at the PBU L-106 site using depressurization-induced dissociation and a single vertical well: reference case (S_{H0} = 0.75).

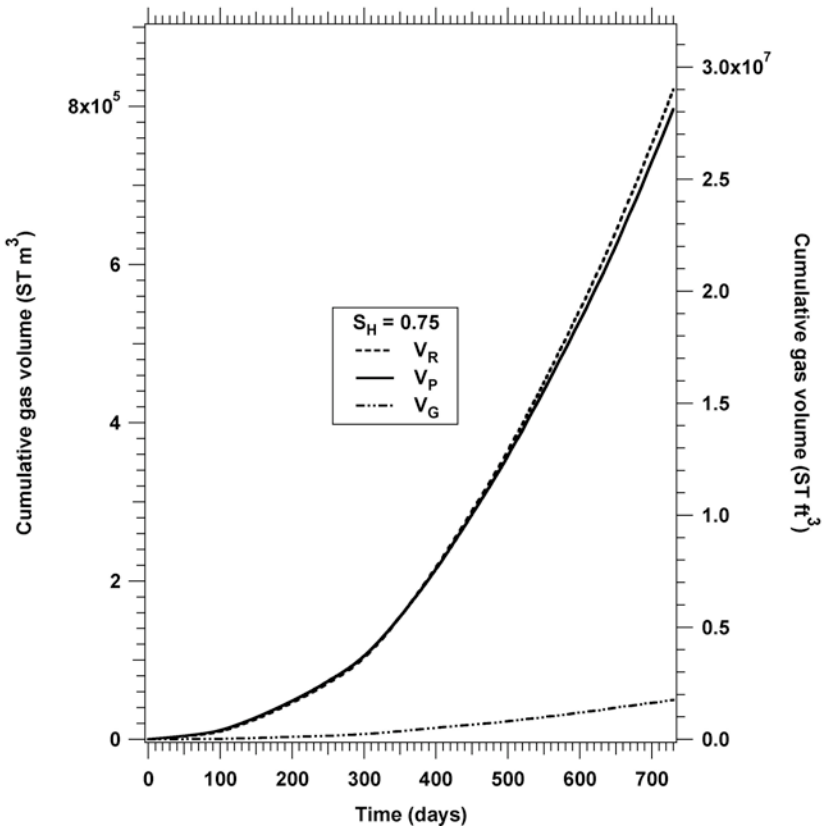

Figure 7 - V_R, V_P and V_F during a proposed long-term production test from the hydrate deposits in the C-Unit at the PBU L-106 site using depressurization-induced dissociation and a single vertical well: reference case (S_{H0} = 0.75).

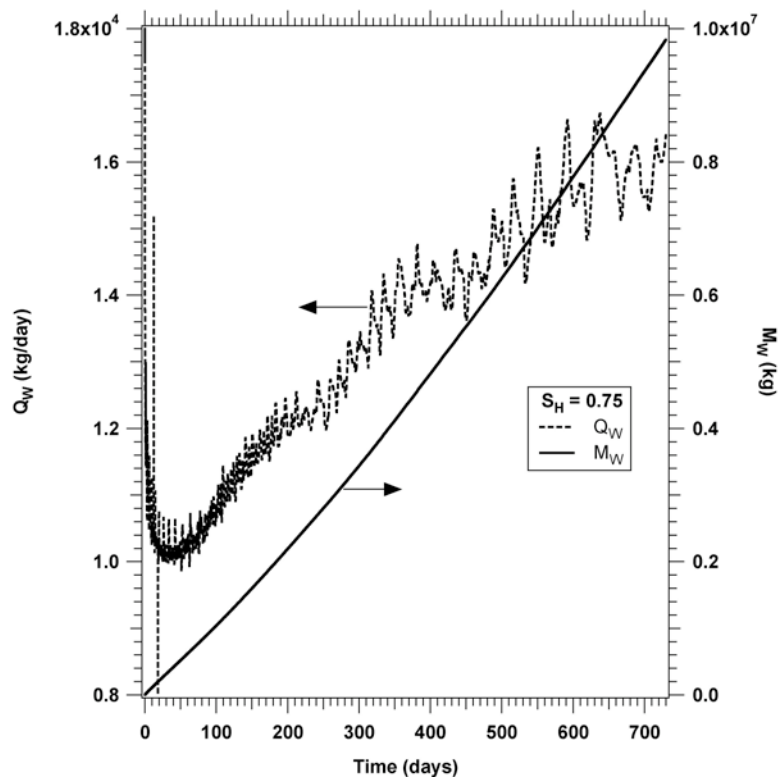

Figure 8 - Q_W and M_W during a proposed long-term production test from the hydrate deposits in C-Unit at the PBU L-106 site using depressurization-induced dissociation and a single vertical well: reference case (S_{H0} = 0.75).

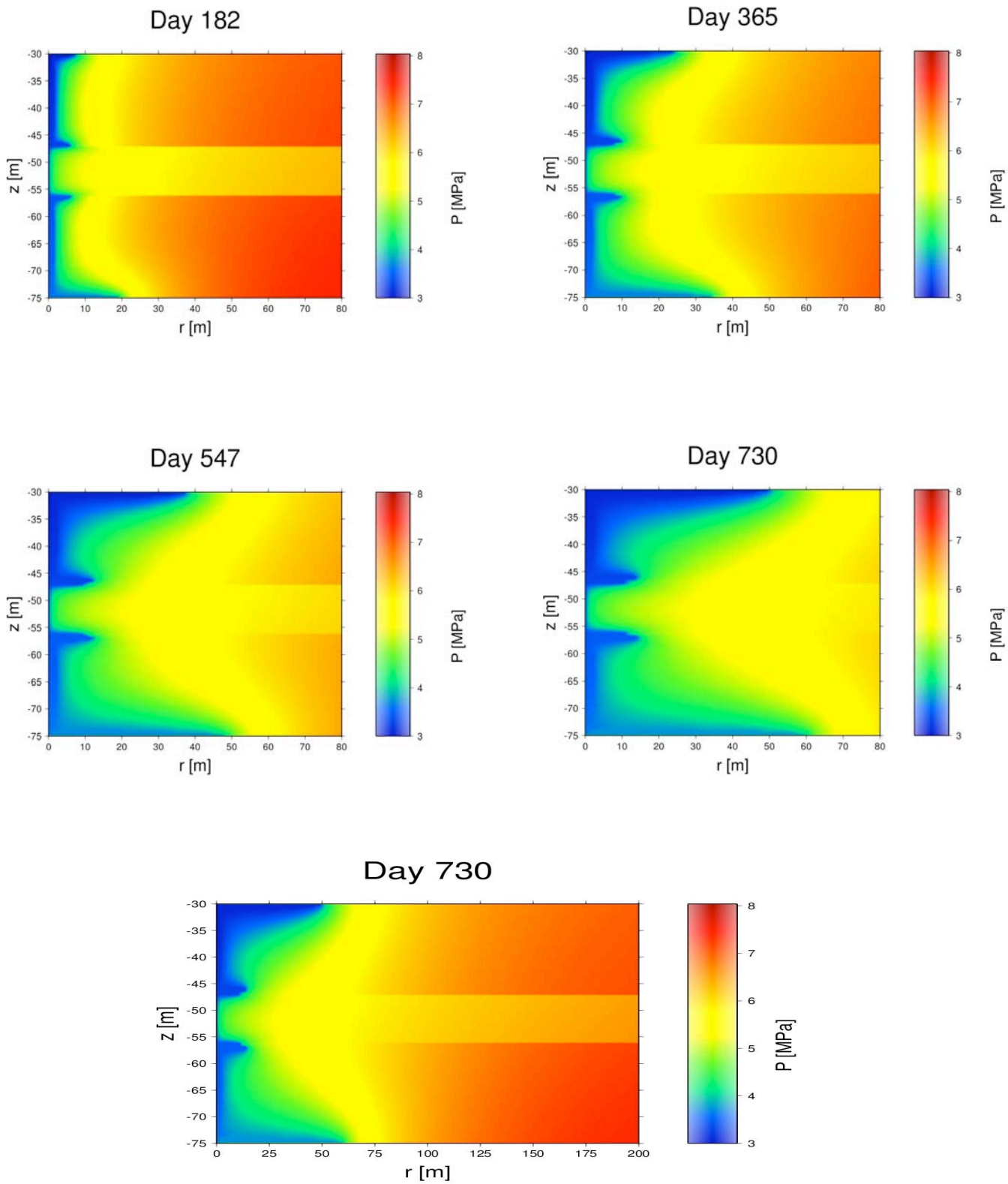

Figure 9 - Evolution of the *P*-distribution over time within *r* = 80 m from the well during a depressurization-based long-term test of gas production from the C-Unit at the PBU L-106 site using a single vertical well (S_{H0} = 0.75).

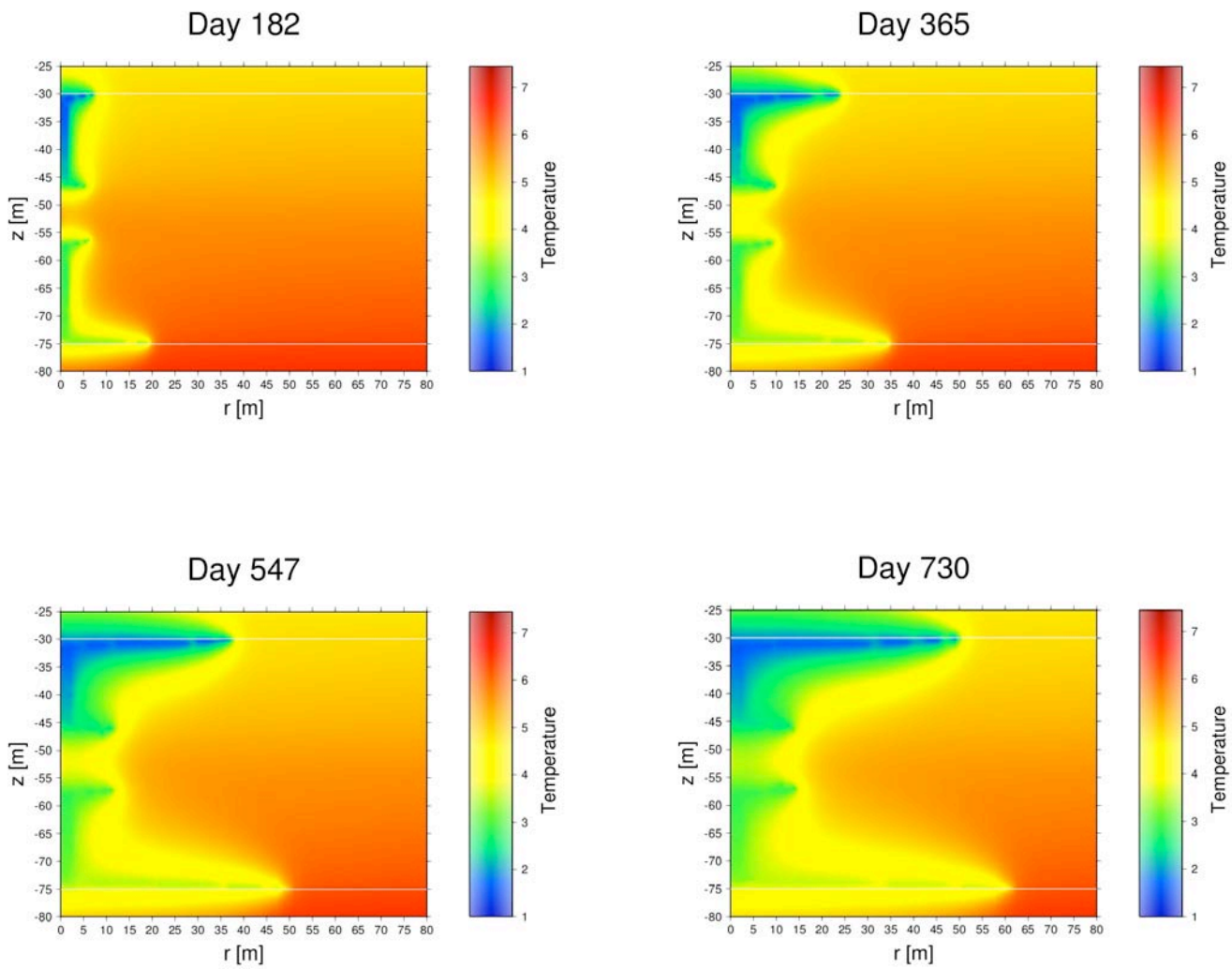

Figure 10 - Evolution of the *T*-distribution over time within *r* = 80 m from the well during a depressurization-based long-term test of gas production from the C-Unit at the PBU L-106 site using a single vertical well (S_{H0} = 0.75).

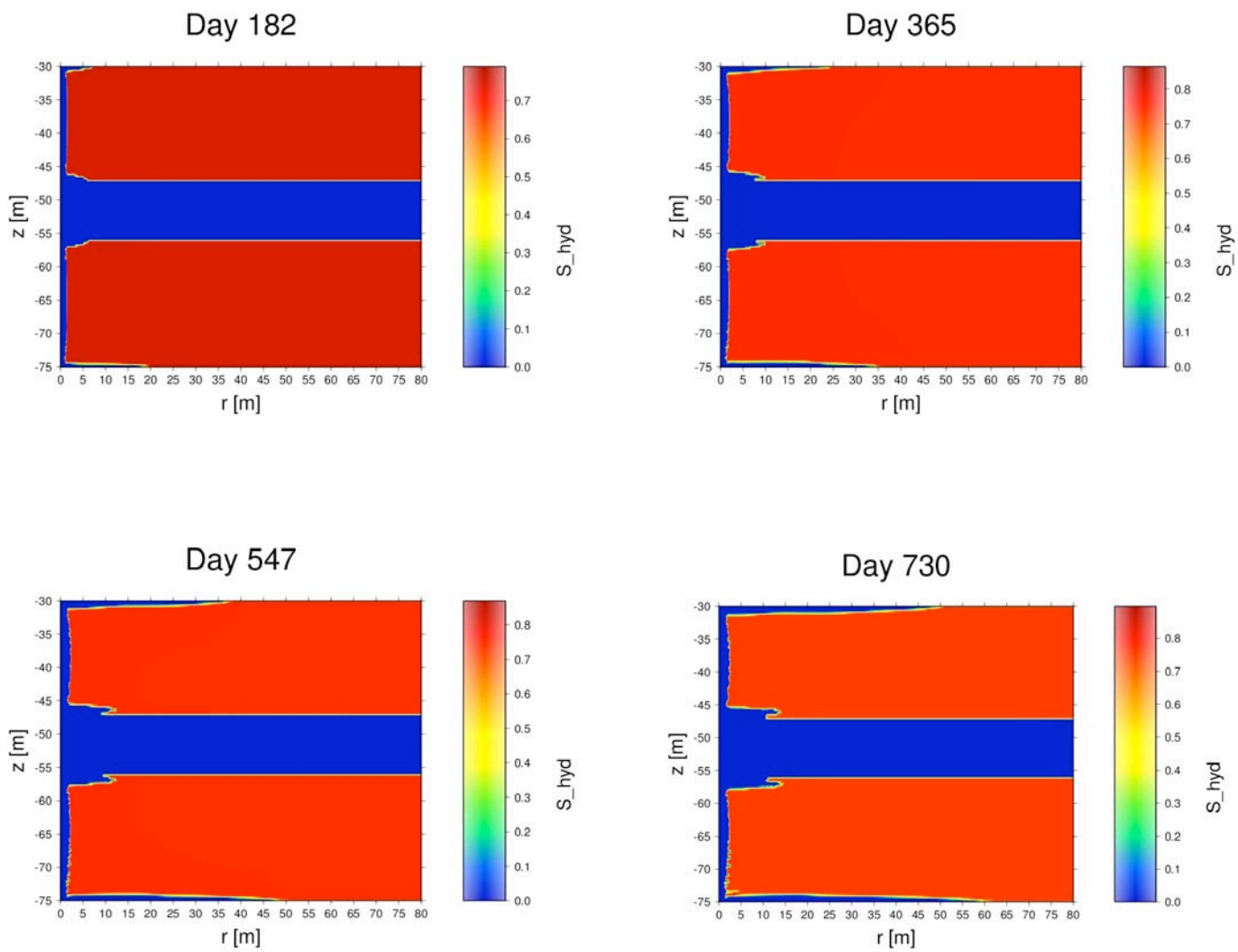

Figure 11 - Evolution of the S_H-distribution over time within r = 80 m from the well during a depressurization-based long-term test of gas production from the C-Unit at the PBU L-106 site using a single vertical well (S_{H0} = 0.75).

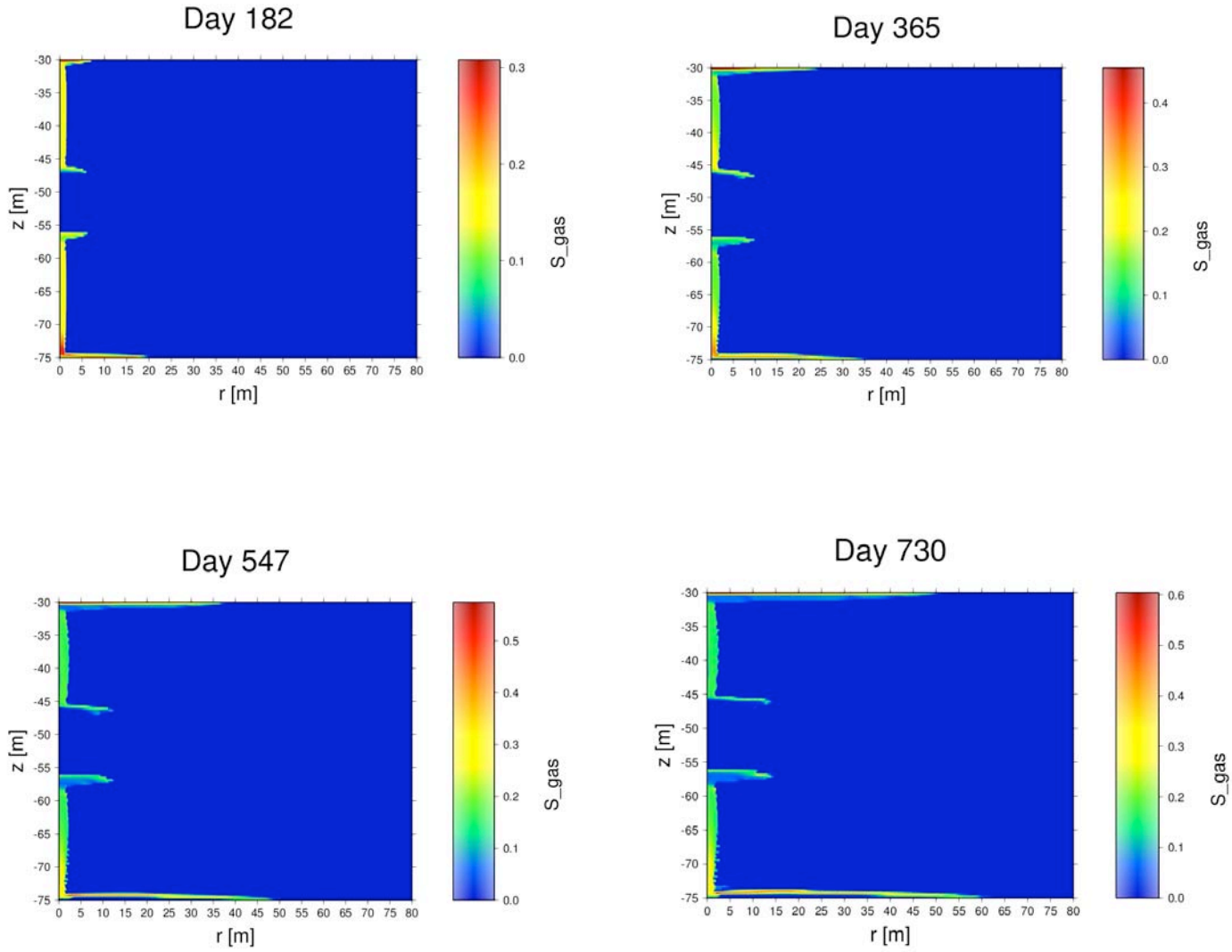

Figure 12 - Evolution of the S_G-distribution over time within r = 80 m from the well during a depressurization-based long-term test of gas production from the C-Unit at the PBU L-106 site using a single vertical well (S_{H0} = 0.75).

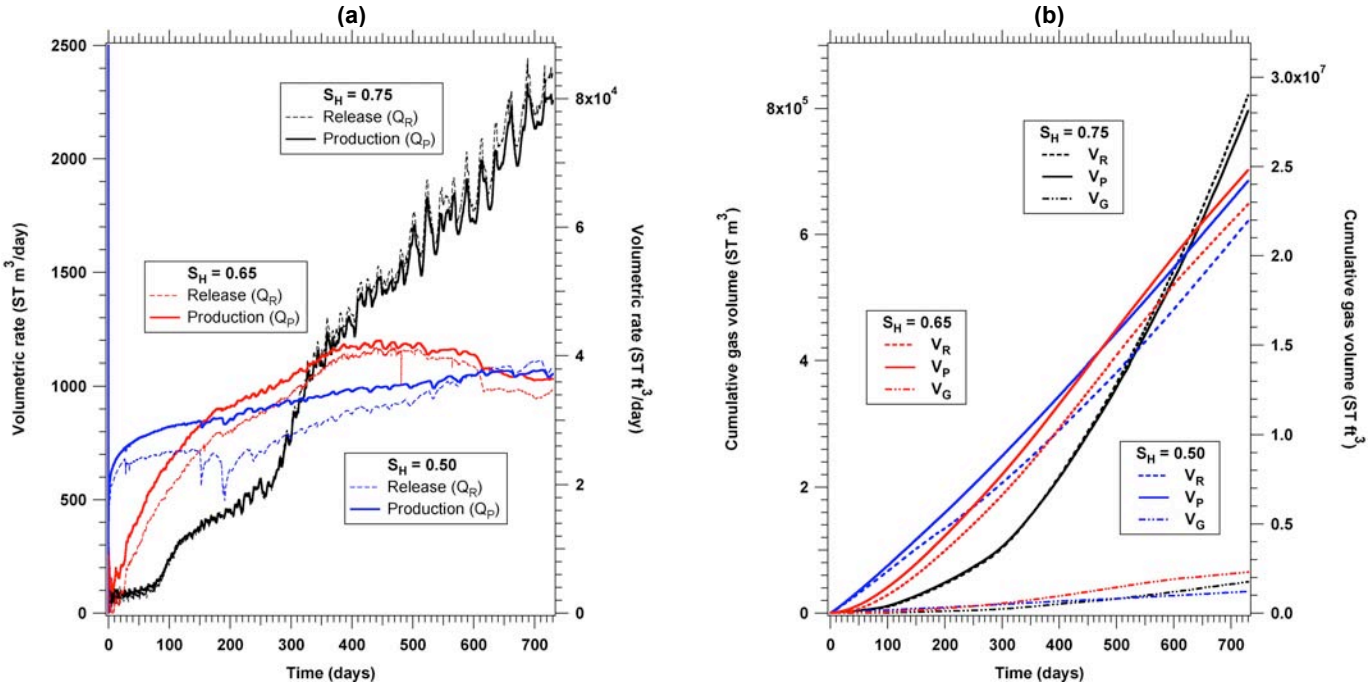

Figure 13 – Effect of S_H on gas production from the C-Unit at the PBU L-106 site using depressurization-induced dissociation and a single vertical well: (a) Q_R and Q_P, and (b) V_R, V_P and V_F.

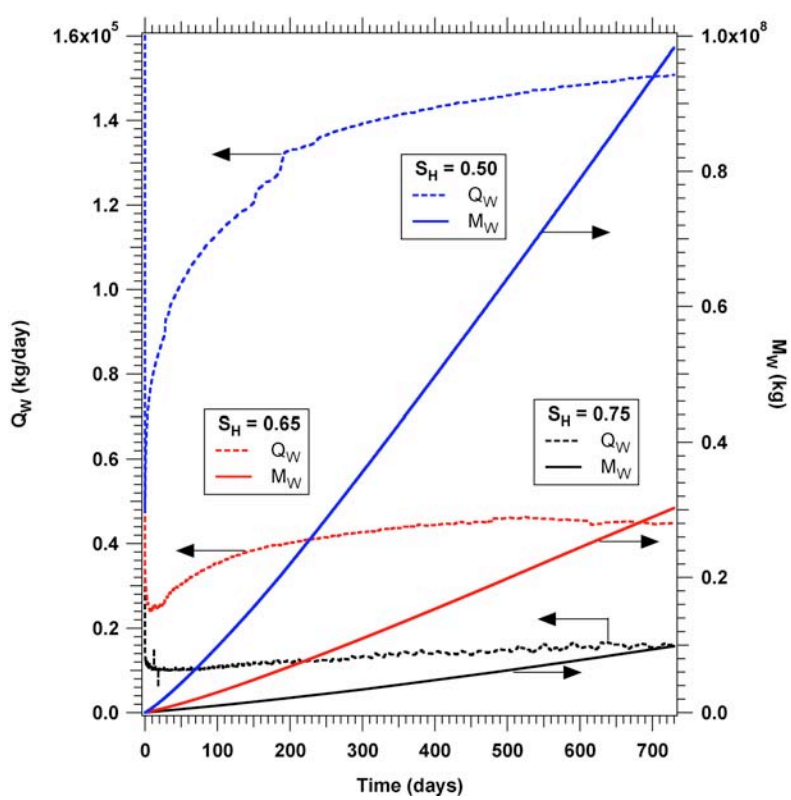

Figure 14 – Effect of S_H on water production (Q_W and M_W) from the C-Unit at the PBU L-106 site during depressurization-based production from hydrates using a single vertical well.

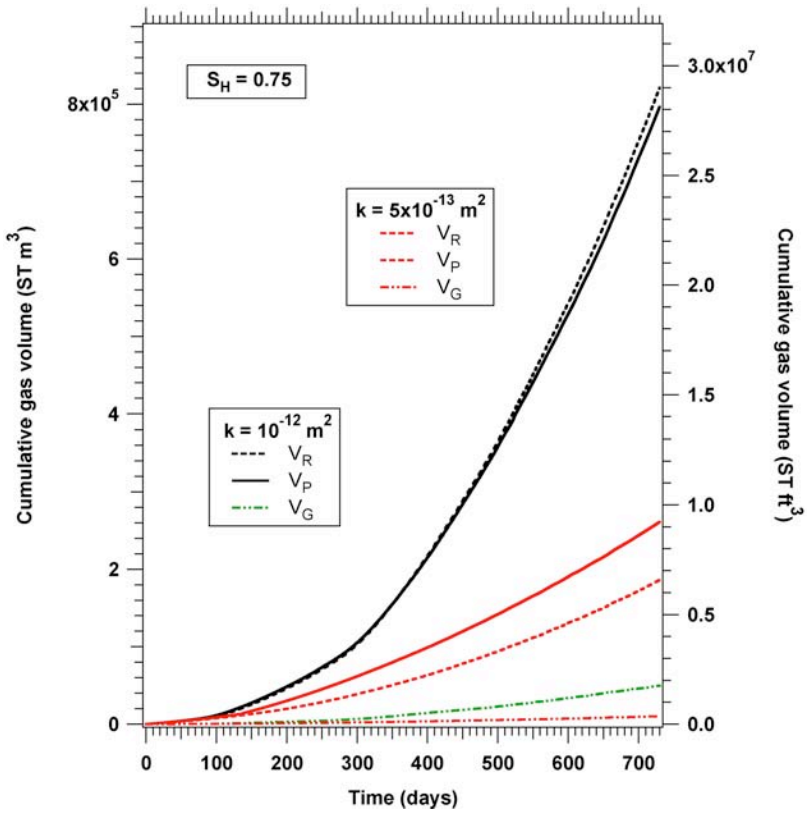

Figure 15 – Effect of intrinsic permeability *k* on gas production (V_R, V_P and V_F) from the C-Unit at the PBU L-106 site using depressurization-induced dissociation and a single vertical well (S_{H0} = 0.75).

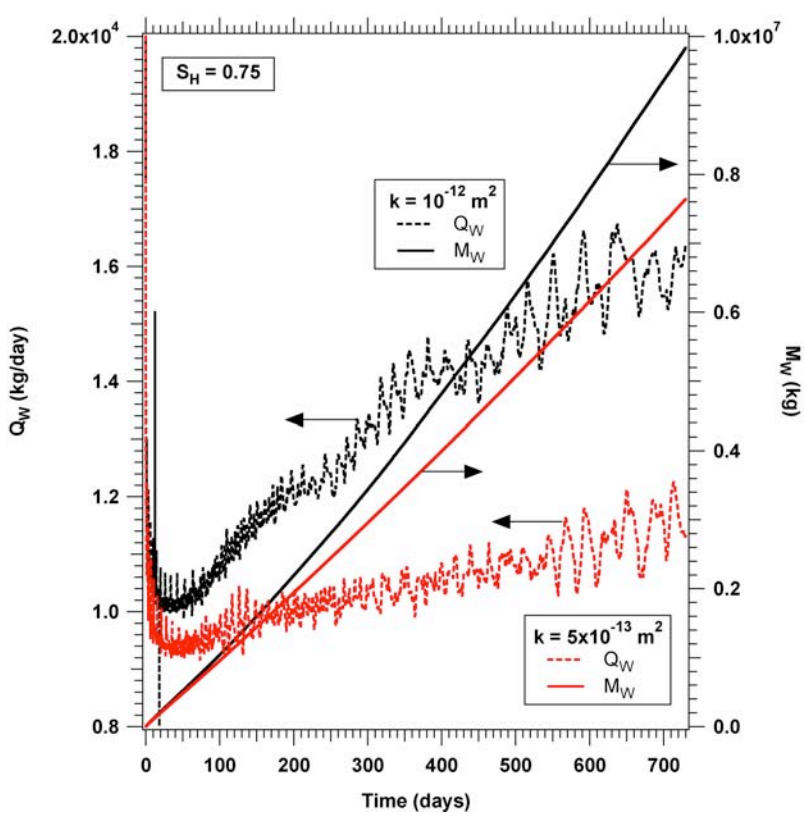

Figure 16 – Effect of intrinsic permeability *k* on water production (Q_W and M_W) from the C-Unit at the PBU L-106 site during depressurization-based production from hydrates using a single vertical well (S_{H0} = 0.75).

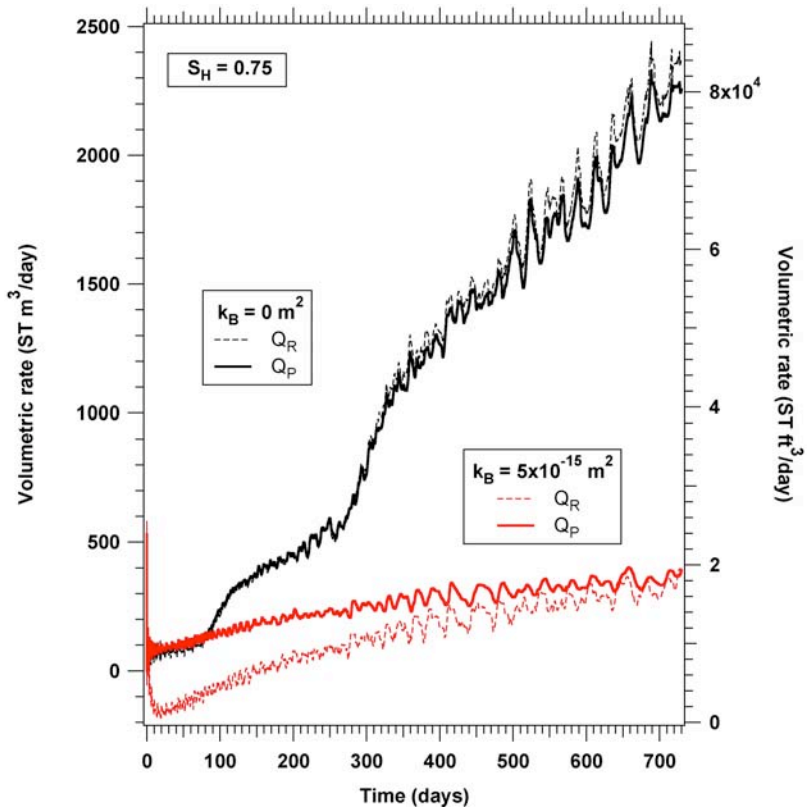

Figure 17 – Effect of the intrinsic permeability of the shale boundaries k_B on gas production (Q_R and Q_P) from the C-Unit at the PBU L-106 site using depressurization-induced dissociation and a single vertical well (S_{H0} = 0.75).

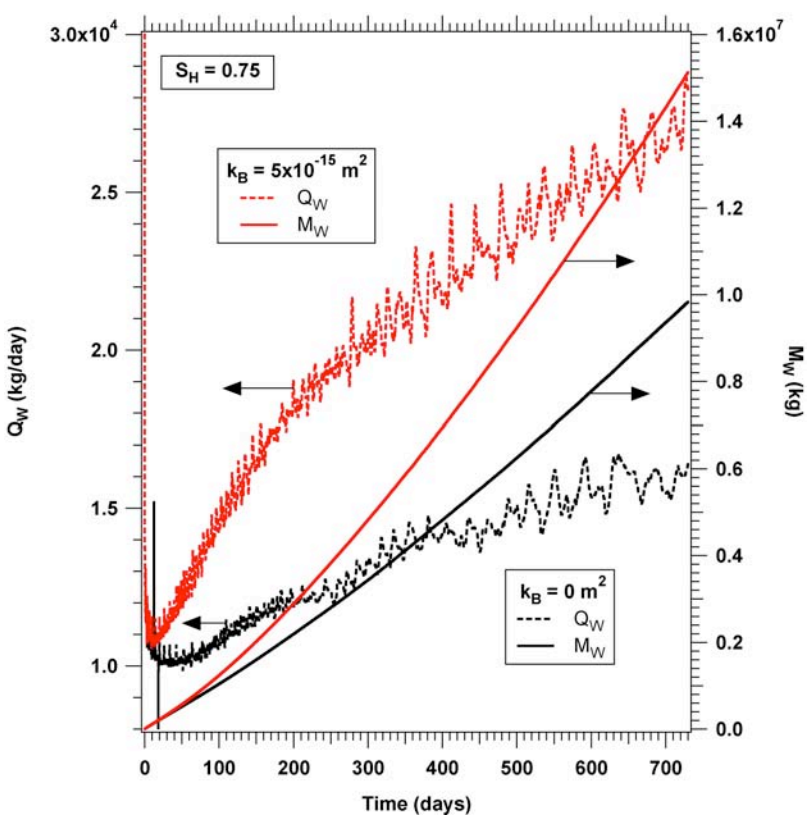

Figure 18 – Effect of intrinsic permeability k on water production (Q_W and M_W) from the C-Unit at the PBU L-106 site during depressurization-based production from hydrates using a single vertical well (S_{H0} = 0.75).

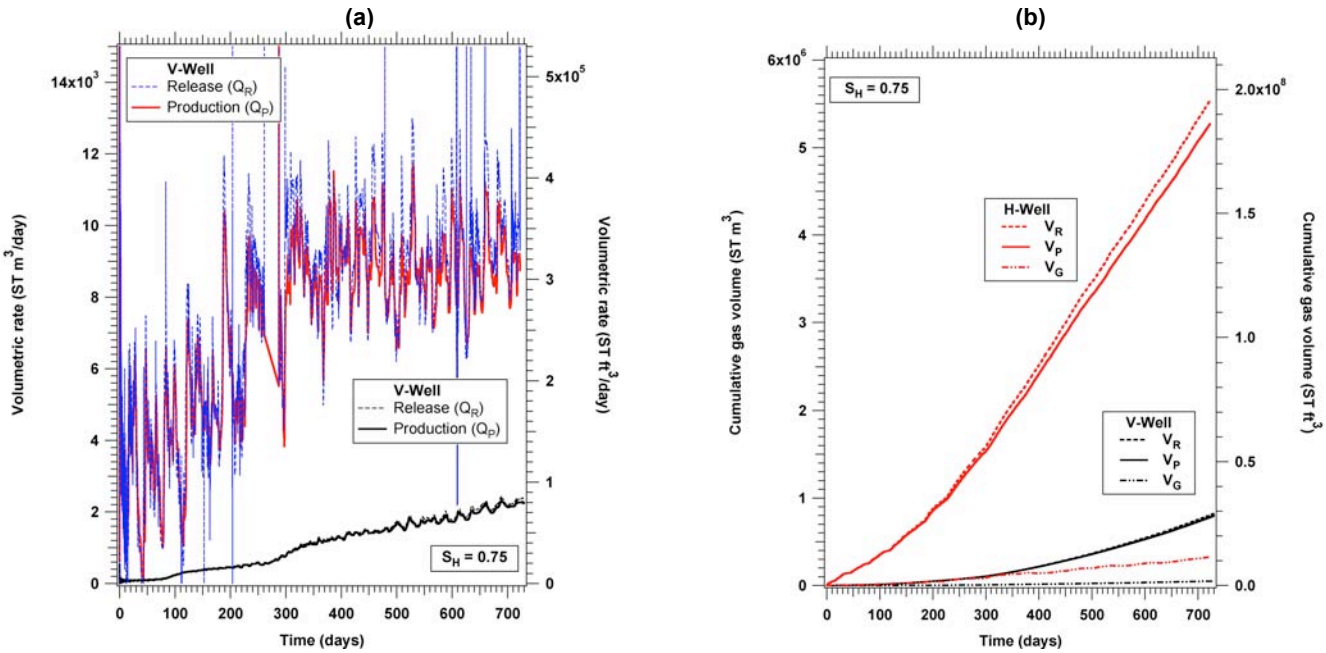

Figure 19 – (a) Q_R and Q_P, and (b) V_R, V_P and V_F describing gas production from the C-Unit at the PBU L-106 site using depressurization-induced dissociation: horizontal vs. a single vertical well (S_{H0} = 0.75).

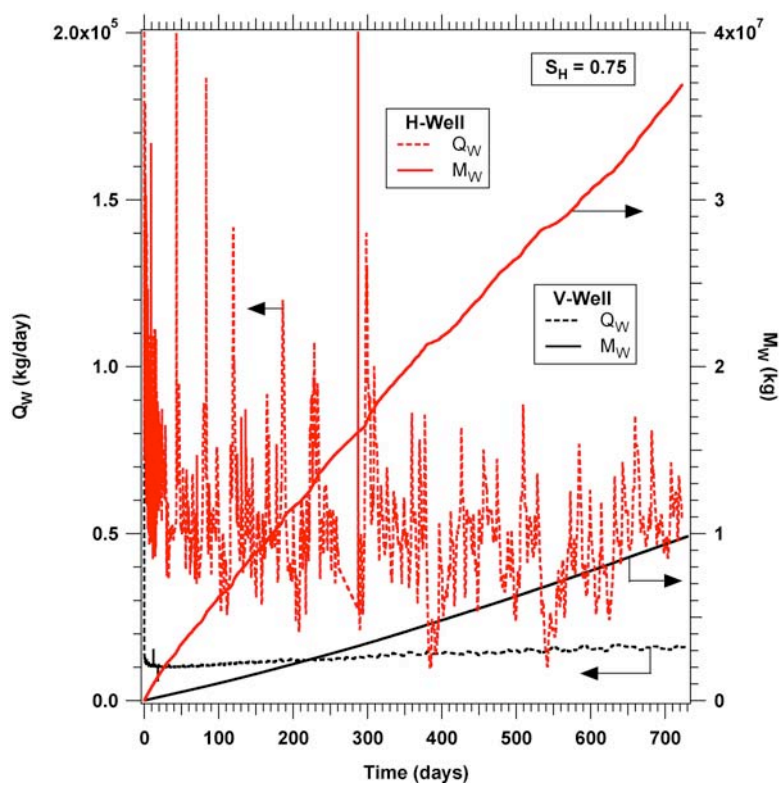

Figure 20 – Water production (Q_W and M_W) from the C-Unit at the PBU L-106 site during depressurization-based production from hydrates: horizontal vs. a single vertical well (S_{H0} = 0.75).

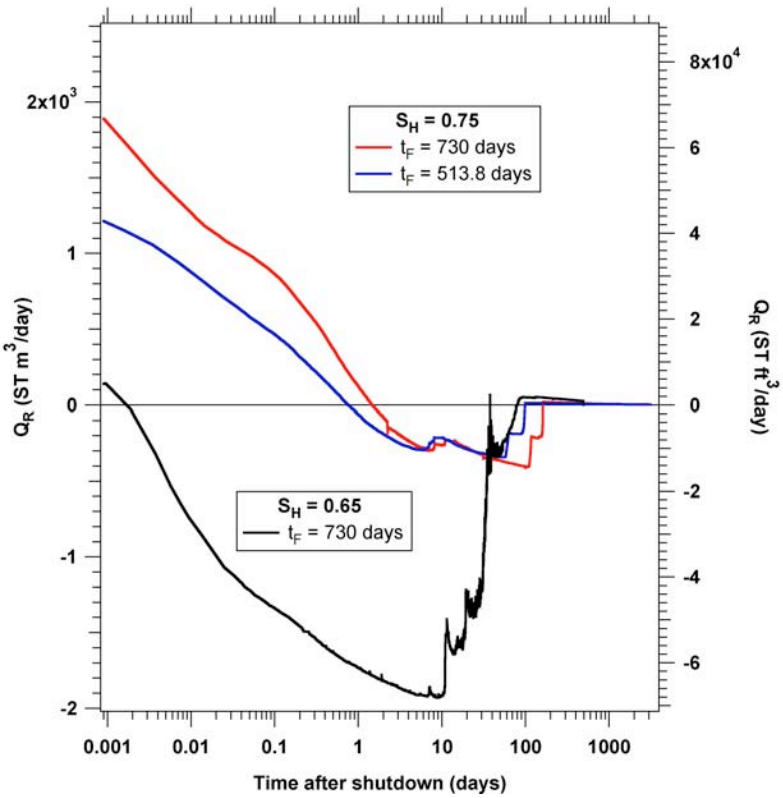

Figure 21 – Response of the C-Unit at the PBU L-106 site to the cessation of production (well shut-in) at a time t_F. (Q_W and M_W) from the C-Unit at the PBU L-106 site during depressurization-based production from hydrates using a single vertical well (S_{H0} = 0.75).

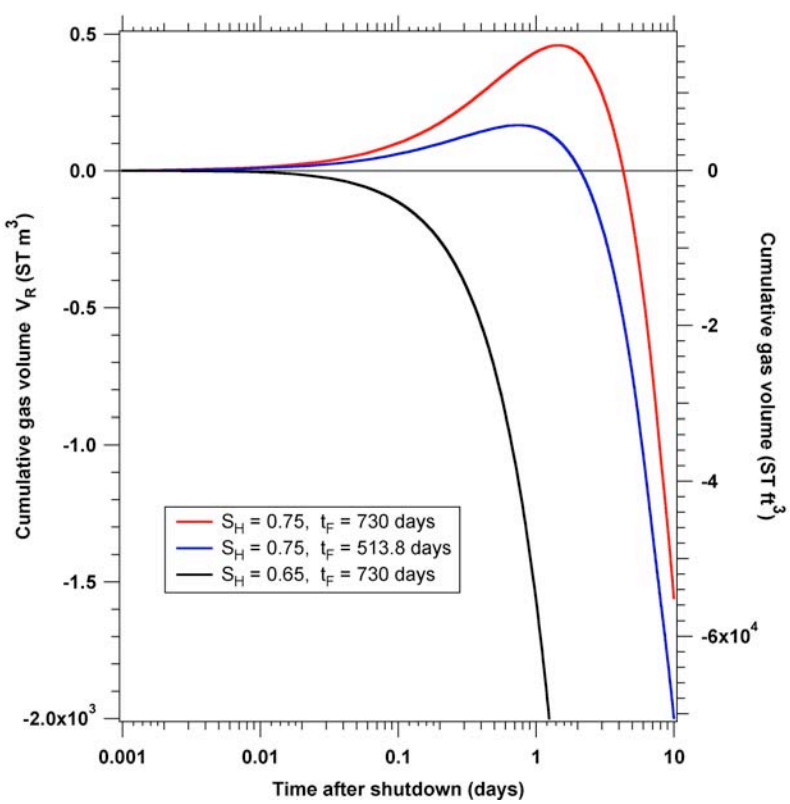

Figure 22 – Early response of the C-Unit at the PBU L-106 site to the cessation of production (well shut-in) at a time t_F. (Q_W and M_W) from the C-Unit at the PBU L-106 site during depressurization-based production from hydrates using a single vertical well (S_{H0} = 0.75).

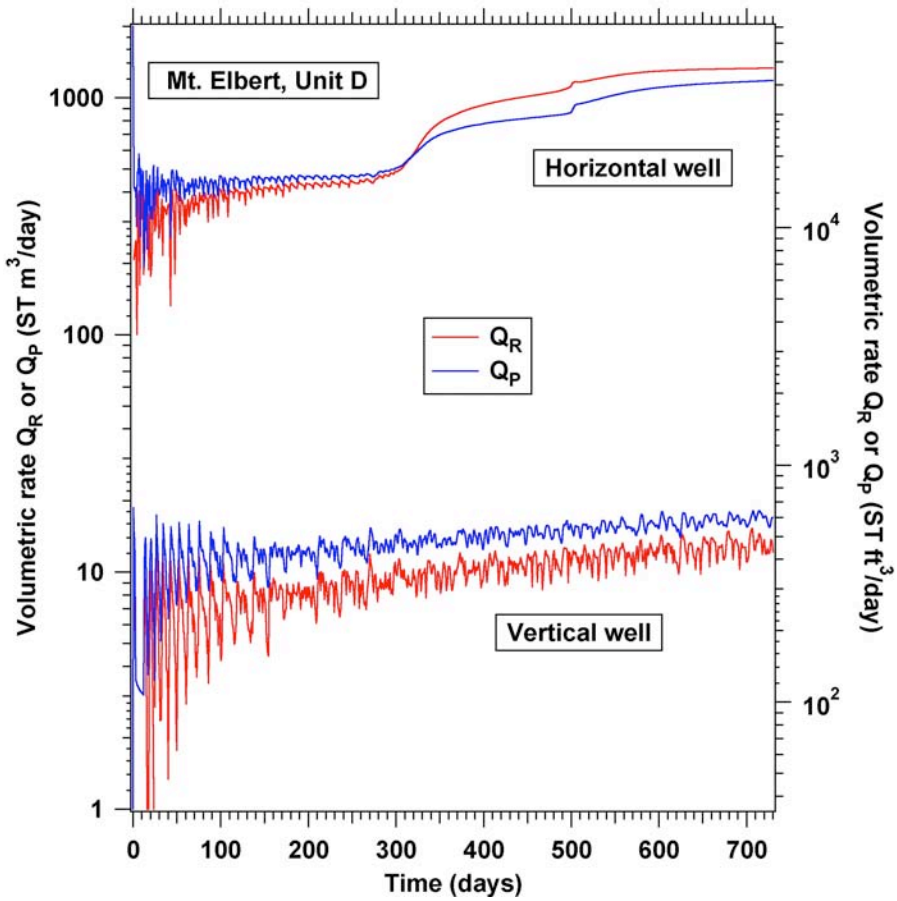

Figure 23 - Q_R and Q_P during a proposed long-term production test from the hydrate deposit in the D-Unit at the Mount Elbert site using depressurization-induced dissociation - horizontal well and a single vertical well (Moridis et al., 2010b).

DISCLAIMER

This document was prepared as an account of work sponsored by the United States Government. While this document is believed to contain correct information, neither the United States Government nor any agency thereof, nor The Regents of the University of California, nor any of their employees, makes any warranty, express or implied, or assumes any legal responsibility for the accuracy, completeness, or usefulness of any information, apparatus, product, or process disclosed, or represents that its use would not infringe privately owned rights. Reference herein to any specific commercial product, process, or service by its trade name, trademark, manufacturer, or otherwise, does not necessarily constitute or imply its endorsement, recommendation, or favoring by the United States Government or any agency thereof, or The Regents of the University of California. The views and opinions of authors expressed herein do not necessarily state or reflect those of the United States Government or any agency thereof or The Regents of the University of California.

Ernest Orlando Lawrence Berkeley National Laboratory is an equal opportunity employer.